frontiers in Earth Science

ORIGINAL RESEARCH
published: 31 March 2021
doi: 10.3389/feart.2021.654136

Occurrence of Irreducible Water and Its Influences on Gas-Bearing Property of Gas Shales From Shallow Longmaxi Formation in the Xishui Area, Guizhou, Southern China

Jian Sun[1,2], Xianming Xiao[1], Qiang Wei[3], Peng Cheng[2] and Hui Tian[2]*

[1] School of Energy Resources, China University of Geosciences (Beijing), Beijing, China, [2] State Key Laboratory of Organic Geochemistry, Guangzhou Institute of Geochemistry, Chinese Academy of Sciences, Guangzhou, China, [3] School of Earth Sciences, East China University of Technology, Nanchang, China

Systematic studies are quite rare on the gas-bearing property and its controlling factors of the shallow Longmaxi shale outside the Sichuan Basin. In a previous study, the gas in place contents of a suit of Longmaxi shale samples with a depth range of 362–394 m from the well XK2, which was drilled in the Xishui area, Guizhou, southern China, were reported. In the present study, the pore structure parameters and irreducible water occurrence characteristics of those samples, and their influences on the gas-bearing property were further investigated. The results show that, compared to the dry sample, the non-micropore specific surface areas and micropore volumes of the moist sample are significantly reduced by an average value of 61 and 30%, respectively, and that the water averagely occupies 82 and 41% of the inorganic and organic non-micropore specific surface areas, respectively, and 44 and 18% of the inorganic and organic micropore volumes, respectively. The shallow shale reservoir is dominated by adsorbed gas. It accounts for 66–93% of the total gas. The water significantly decreases the adsorption capacity of the inorganic matte (mainly clay minerals) pores, but has a limited influence on that of the organic matter pores. The adsorbed gas occurs mostly in the organic matter nanopores, and even if the shales were highly saturated with the water, they can still store a certain amount of the adsorbed gas. These results are to provide some guides for the evaluation and exploration of the shallow Longmaxi shale located in the strongly tectonic transformation areas of southern China.

Keywords: Longmaxi formation, shallow shale, irreducible water, pore structure, gas-bearing property, adsorbed gas

OPEN ACCESS

Edited by:
Dawei Lv,
Shandong University of Science and Technology, China

Reviewed by:
Qingyong Luo,
China University of Petroleum, China
Xianfeng Tan,
Chongqing University of Science and Technology, China

****Correspondence:***
Xianming Xiao
xmxiao@cugb.edu.cn

Specialty section:
This article was submitted to Economic Geology, a section of the journal Frontiers in Earth Science

Received: *15 January 2021*
Accepted: *08 March 2021*
Published: *31 March 2021*

Citation:
Sun J, Xiao XM, Wei Q, Cheng P and Tian H (2021) Occurrence of Irreducible Water and Its Influences on Gas-Bearing Property of Gas Shales From Shallow Longmaxi Formation in the Xishui Area, Guizhou, Southern China. Front. Earth Sci. 9:654136. doi: 10.3389/feart.2021.654136

Abbreviations: ρ_b, density of free gas; ρ_{sample}, apparent density of the shale; BET, Brunauer-Emmett-Teller; BJH, Barrett-Joyner-Halenda; DA, Dubinin-Astakhov; DFT, Density Functional Theory; GBP, gas-bearing property; GIP, gas in place; IM, inorganic matter; M, average molar mass; OM, organic matter; P/P_0, relative pressure; PSD, pore-size distribution; Q_{ads}, adsorbed gas content; Q_{free}, free gas content; Q_{total}, total gas content; R^2, correlation coefficient; S_{BET}, specific surface area; S_{BET-IM}, BET surface area of inorganic matter; S_{BET-OM}, BET surface area of organic matter; S_W, water saturation; TOC, total organic carbon; V_{mic}, micropore volume; V_{mic-IM}, inorganic matter micropore volume; V_{mic-OM}, organic matter micropore volume.

INTRODUCTION

Shale gas, mainly stored as free and adsorbed states, is a typical unconventional natural gas (Jarvie et al., 2007; Bustin et al., 2008; Ross and Bustin, 2009). For different shale reservoirs, not only do their gas contents vary greatly, but the percentages of the adsorbed and free gasses can differ widely. For examples, the percentages of adsorbed gas in the Barnett and Lewis shales (United States) are approximately 20% and in a range of 60–85%, respectively (Curtis, 2002), and the free gas percentage of Longmaxi shale samples from the Jiaoshiba Block in the Sichuan Basin, varies from 60 to 75% (Dong et al., 2014). The gas-bearing property (GBP) and gas in place (GIP) content of shales are not only related to their geological conditions (temperature and pressure), but also restricted by their geochemical properties. For a specific gas shale, the free gas content is mainly related to its porosity, gas saturation, and geological temperature and pressure (Bustin et al., 2008; Gasparik et al., 2012; Pan and Connell, 2015; Ye et al., 2016; Zhang Y. S. et al., 2020), but the controlling mechanism of the adsorbed gas is more complex. Except for the factors mentioned above, the adsorbed gas content is also correlated with its pore type, property and structure, which are comprehensively controlled by the organic matter content and type, mineral composition, and thermal maturity (Yang and Aplin, 1998; Dewhurst et al., 1999; Chalmers and Bustin, 2007, 2008; Ross and Bustin, 2007; Curtis et al., 2010, 2011; Song et al., 2013; Zhang et al., 2013; Shan et al., 2017; Chen et al., 2018; Hou et al., 2018; Li et al., 2018; Bhowrnik and Dutta, 2019; Klewiah et al., 2019; Wang and Guo, 2019; Gou et al., 2020; Zhang Y. F. et al., 2020). High-pressure adsorption experiments based on dry samples are generally carried out to evaluate the adsorption capacity of the targeted shales. The achieved results show that, for high and over mature shales, nanopores are extremely developed in their OM (organic matter), and the TOC (total organic carbon) content presents an obvious positive linear relation to the adsorption capacity (Chalmers and Bustin, 2008; Ross and Bustin, 2009; Gasparik et al., 2012, 2014; Tan et al., 2014; Pan et al., 2016; Tian et al., 2016; Fu, 2017; Wang and Guo, 2019), with a R^2 (correlation coefficient) of 0.67–0.99 (Pan et al., 2016; Fu, 2017). Moreover, clay minerals can also have some gas adsorption capacities to methane (Aringhieri, 2004; Sondergeld et al., 2010; Curtis et al., 2011; Ji et al., 2012; Gasparik et al., 2014; Chen et al., 2016). According to the methane adsorption experiments carried out by Ji et al. (2012), kaolinite, chlorite, and illite could adsorb methane with an amount up to 2.5, 2.3, and 1.8 m^3/t, respectively.

Shale reservoirs always have some water in their pore system (Li et al., 2016a; Hu et al., 2018). Recently, quite a few papers have been related to the occurrence characteristics and mechanism of the pore water in gas shales and its influences on their adsorption capacities (Chalmers and Bustin, 2008; Ross and Bustin, 2009; Gasparik et al., 2014; Chen et al., 2016; Li et al., 2016b; Liu et al., 2018; Bai et al., 2020; Wang et al., 2020). The results imply that water can coexist in non-micropores and micropores in absorbed and condensed states, respectively (Newsham et al., 2003; Charriere and Philippe, 2010), and distributes in both OM and IM (inorganic matter) pores (Cheng et al., 2017, 2018), which significantly reduces the methane adsorption capacity (Ross and Bustin, 2009; Gasparik et al., 2014). Nevertheless, those findings are mainly obtained from the laboratory data, with determination results calculated from relevant theoretical models for samples with different water saturations derived from equilibrium water adsorption experiments (Chareonsuppanimit et al., 2012; Gasparik et al., 2012, 2014; Ji et al., 2012; Zhang et al., 2012; Yaguzhinsky et al., 2013), lacking the constraint and validation of data from geological gas shales (Li et al., 2016b).

After the commercial development of the Longmaxi shale gas in the Sichuan Basin, southern China (Li and Zhang, 2015; Guo, 2016), the exploration of shallow marine shale gas outside the Sichuan Basin has made significant progresses. For instance, the GIP content of the Longmaxi shale in the Zhaotong Block, Yunnan Province can reach 3.81 m^3/t, with an initial gas production of 0.39–1.12 $\times$ 10^4 m^3/d although its burial depth is less than 1,000 m (Tian, 2018; Yang, 2018; Liang et al., 2020). The shallow marine shale gas in southern China is expected to become a new exploration field (Li, 2018; Liang et al., 2020).

The shallow Longmaxi shale in northern Guizhou develops widely, and is expected to have a huge amount of shale gas resources (Liang et al., 2008; Li et al., 2012; Hu et al., 2014). Sun et al. (2020) reported the data of geochemistry and GIP contents of a suit of Longmaxi shale samples taken from the well XK2 in this area, and revealed that the shallow Longmaxi shale really contains a high content of shale gas. On the basis of the previous work, the pore structures of those shale samples under the moist and dry conditions were analyzed, respectively, the pore water occurrence characteristics in nanopores were investigated, and the influences of them on the GBP were discussed.

MATERIALS AND METHODS

Samples

There are totally sixteen Longmaxi shale samples investigated in this study, which were collected from the well XK2 in northern Guizhou, southern China (**Figure 1**). The collection and preparation methods of those samples, and their geochemical characteristics, pore water contents and total porosity were reported by Sun et al. (2020) and are briefly summarized here. The 16 shale core samples (with a depth interval of 362–394 m) were collected at an interval of about 2 m. Each sample was quickly divided into two parts. One part was immediately conducted on the GIP content test, and the other part was sealed in plastic bags and sent to the laboratory for the analysis of the pore water content, TOC content, mineral composition, total porosity (Sun et al., 2020). The pore water content of the studied shale samples was measured by the oven-drying and weight-loss method, each sample was drilled from its middle to obtain a small cylinder sample (15 mm in diameter and 20 mm in length). The shale TOC content was measured by a LECO CS-230 carbon-sulfur analyzer, the samples were crushed into powders of 80 mesh sizes. X-ray diffraction (XRD) analysis of the sample powders (200 mesh) was carried out using a Bruker D8 Advance X-ray diffractometer. The total porosity was determined by the differences between the shale skeletal density

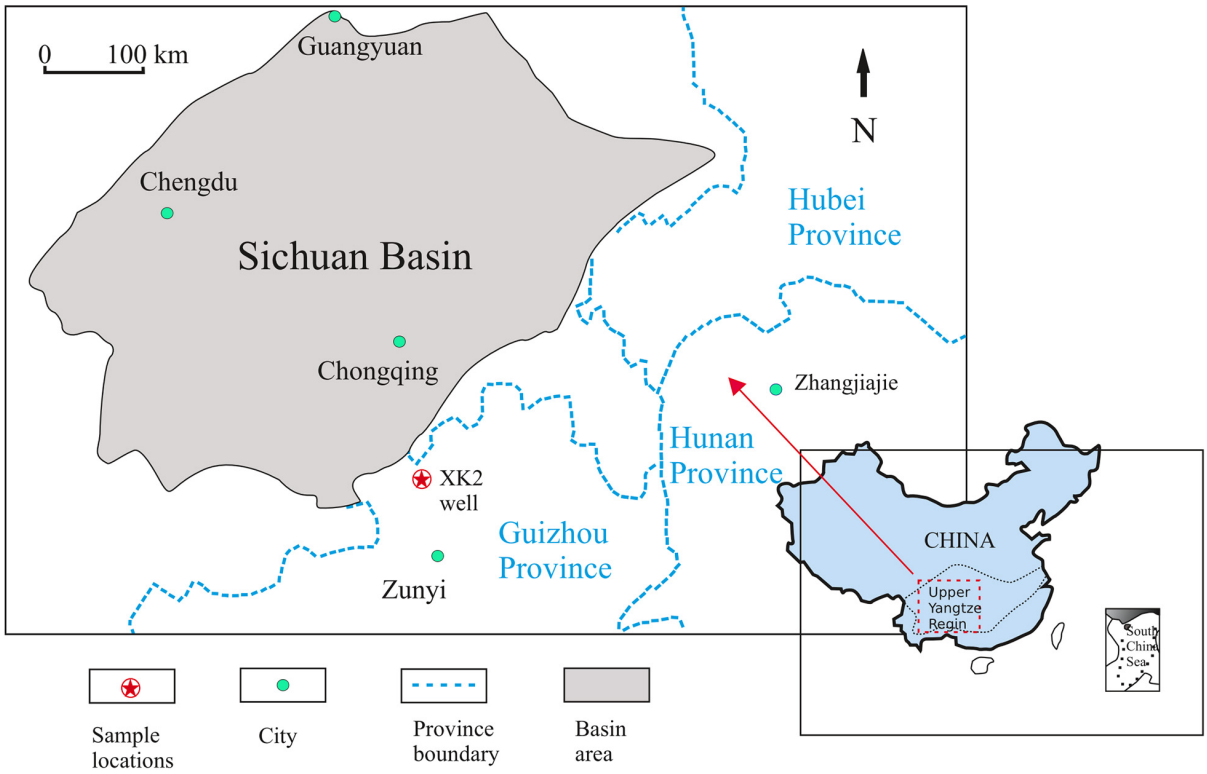

FIGURE 1 | Map showing the location of the well XK2 [modified from Cheng et al. (2018)].

and the apparent density, the two densities were measured with a helium pycnometer (Ultrapyc 1200e) and a hydrometer (DAHO-120M), respectively.

The samples have the TOC, clay mineral, quartz, and carbonate mineral contents of 1.50–8.04%, 20.70–57.00%, 25.00–60.00%, and 4.80–15.80%, respectively, with the porosity of 3.03–5.50% (**Table 1**). The measured pore water content of those samples is between 5.01 and 12.38 mg/g (**Table 1**). It was deemed to be the connate irreducible water content by Sun et al. (2020). This is because the samples were taken from a gas-bearing shale stratum with an ultra-low water saturation, and the gas in the shales prevented the inflow of outside water during the drilling and sampling processes. Therefore, it should be kept in mind that the pore water content of the studied samples can be basically representative for that in their reservoir conditions.

Low Pressure N_2 and CO_2 Adsorption Experiments

The non-micropore (mesopore + macropore) and micropore structures of the moist and dry shale samples were tested using low-pressure N_2 and CO_2 adsorption experiments, respectively, by a Micromeritics ASAP 2020 apparatus. The main experimental methods are summarized below. The samples were crushed into 20–40 meshes (380–830 μm), and each sample was prepared into two parts. One part retained the irreducible water (i.e., the moist sample), and the other part was dried in a vacuum oven for 12 h at a temperature of 110℃ to remove the water and/or volatile substances (i.e., the dry sample). For the dry sample, loaded approximately 1 g into sample tube for further degassing under the high vacuum conditions (<10 mmHg) at 110°C for 12 h in degassing station of the apparatus, and then it was moved to the analysis station for the adsorption experiment. The moist sample was directly placed in the analysis station for the freezing, degassing and adsorption experiments. The samples were tested at a P/P_0 (the relative pressure) of 0.005–0.995 and a liquid nitrogen temperature of 77.35 K for the N_2 adsorption, and at a P/P_0 of 1×10^{-5}–0.03 and a temperature of 273.15 K (ice-water mixture environment) for the CO_2 adsorption. For the N_2 adsorption, the adsorption and desorption isotherms were tested to analyze the type of hysteresis. According to the N_2 adsorption isotherms, the modified BET (Brunauer-Emmett-Teller) equation was utilized to determine the non-micropore specific surface area (Brunauer et al., 1938; Gregg and Sing, 1982; Tian et al., 2015), and the BJH (Barrett-Joyner-Halenda) model was adopted to determine the non-micropore pore-size distribution (PSD) (Barrett et al., 1951; Tian et al., 2013; Pan et al., 2015) for the dry and moist samples. The micropore volume was determined by DA (Dubinin-Astakhov) equation (Dubinin, 1989; Clarkson and Bustin, 1999; Ross and Bustin, 2009; Cheng et al., 2017), and the DFT (Density Functional Theory) was utilized calculating the micropore PSD on the basis of the CO_2 adsorption data from the both sample sets (Mastalerz et al., 2013; Lin et al., 2014).

TABLE 1 | Data of geochemistry, mineral composition, and pore water content of the studied shale samples.

Sample ID	Depth (m)	TOC (%)	Pore water (mg/g)	Apparent density (g/cm^3)	Porosity (%)	Mineral composition (%)				
						Quartz	Feldspar	Total clays	Total carbonates	Pyrite
JX-1	362.61	1.50	8.02	2.64	3.03	30.60	16.00	47.00	4.80	1.60
JX-2	366.90	2.37	10.96	2.63	3.42	27.40	12.20	51.60	7.60	1.40
JX-3	370.04	2.72	12.38	2.60	3.96	25.00	8.50	57.00	7.30	2.00
JX-4	375.06	4.38	8.60	2.51	4.10	33.80	7.30	46.10	10.90	2.00
JX-5	376.78	4.15	8.24	2.50	4.39	36.30	9.90	39.20	12.00	2.50
JX-6	377.51	3.78	8.46	2.50	4.20	35.00	12.20	38.80	11.70	2.40
JX-7	381.70	3.73	5.01	2.50	3.84	53.90	5.60	25.20	13.10	2.30
JX-8	383.56	3.61	6.20	2.50	4.20	45.50	10.20	31.80	10.10	2.50
JX-9	385.26	4.48	5.44	2.48	3.63	56.30	6.60	20.70	14.00	2.30
JX-10	387.52	4.25	5.21	2.51	3.59	57.70	6.20	21.00	10.50	4.70
JX-11	388.89	4.97	6.50	2.47	4.15	50.10	7.80	28.60	10.60	2.80
JX-12	390.48	5.48	5.44	2.49	4.42	52.50	7.60	26.60	8.00	5.30
JX-13	391.92	7.07	5.56	2.39	4.63	60.00	8.70	23.10	6.40	1.90
JX-14	392.36	8.04	6.17	2.43	5.41	41.40	8.40	36.70	12.10	1.50
JX-15	393.03	6.47	6.85	2.41	4.96	53.90	4.50	22.30	15.80	3.50
JX-16	394.01	7.81	10.36	2.43	5.50	34.10	10.40	40.20	15.50	2.90

Data are cited from Sun et al. (2020).

Calculation of Water Saturation

According to the pore water content, porosity and apparent density data of the shale samples from the well XK2 (**Table 1**), their water saturation (S_W, %) can be determined by Eq. 1:

$$S_W = \frac{C_{IW}\ \rho_{sample}}{10\ \Phi\ \rho_w} \quad (1)$$

where C_{IW} is the pore water content (mg/g); Φ is the porosity (%); ρ_{sample} is the apparent density (g/cm^3); ρ_w is the pore water density (g/cm^3), and it is supposed that its density is 1 g/cm^3 for all samples.

Calculation of the Shale Free and Adsorbed Gas Contents

According to the shale gas composition from the well XK2 reported by Sun et al. (2020), the shale gas from the XK2 well shale samples consists of CH_4, C_2H_6, and CO_2 with an average content of 93.99, 1.21, and 4.80%, respectively, while other gasses, such as C_3, N_2 and so on were not detected due to their negligible contents. Thus, the average molar mass (M) of the shale gas was calculated using Eq. 2. The free gas density (ρ_b) was obtained by a PVTsim software. Combined with the porosity, water saturation and apparent density data, the free gas content (Q_{free}) was determined using Eq. 3. The adsorbed gas content (Q_{ads}) was obtained by the difference between the total gas content (Q_{total}) (i.e., the GIP content) and the Q_{free} (Eq. 4). These equations are as follows:

$$M = aM_1 + bM_2 + cM_3 \quad (2)$$

$$Q_{free} = \frac{22400\Phi\ (1 - S_w)\ \rho_b}{M\rho_{sample}} \quad (3)$$

$$Q_{ads} = Q_{total} - Q_{free} \quad (4)$$

where M is the average molar mass of the shale gas (g/mol); Q_{free}, Q_{ads}, and Q_{total} are the free, adsorbed, and total gas contents, respectively (m^3/t); M_1, M_2, and M_3 are the molar mass of CH_4, C_2H_6 and CO_2, respectively (g/mol); a, b, and c are the volume percentages of CH_4, C_2H_6, and CO_2, respectively (%); ρ_b is the free gas density (g/ml), and it can be determined using a PVTsim software based on the reservoir temperature, pressure, and gas composition data.

RESULTS AND DISCUSSION

Pore Structures of the Moist and Dry Samples

Low Pressure N_2 Adsorption and Pore Distribution

Figure 2 displays the isotherms of N_2 adsorption and desorption of the dry and moist samples. It should be noted that the N_2 adsorption and desorption of the studied 16 shale samples are mainly controlled by their TOC contents, the selected 8 samples in **Figure 2** form a TOC gradient, and can reflect the characteristics of the whole sample set (same in **Figures 3–5** below). **Figure 2** indicates that the adsorption quantity of the moist sample is definitely less than that of its corresponding dry sample. Furthermore, the isotherm shapes of the dry and moist samples are significantly different. For the dry sample, the isotherm of N_2 adsorption is very close to the type II isotherm according to the IUPAC (International Union of Pure and Applied Chemistry) (Brunauer et al., 1940; Sing et al., 1985; Rouquerol et al., 1994). It shows a distinct hysteresis loop, without plateau at the p/p_0 approximately 1, and a notable adsorption quantity, besides, can be seen at the lowest p/p_0 (<0.01), implying that the mesopore, macropore, and micropore are well developed in the dry sample (Sing et al., 1985).

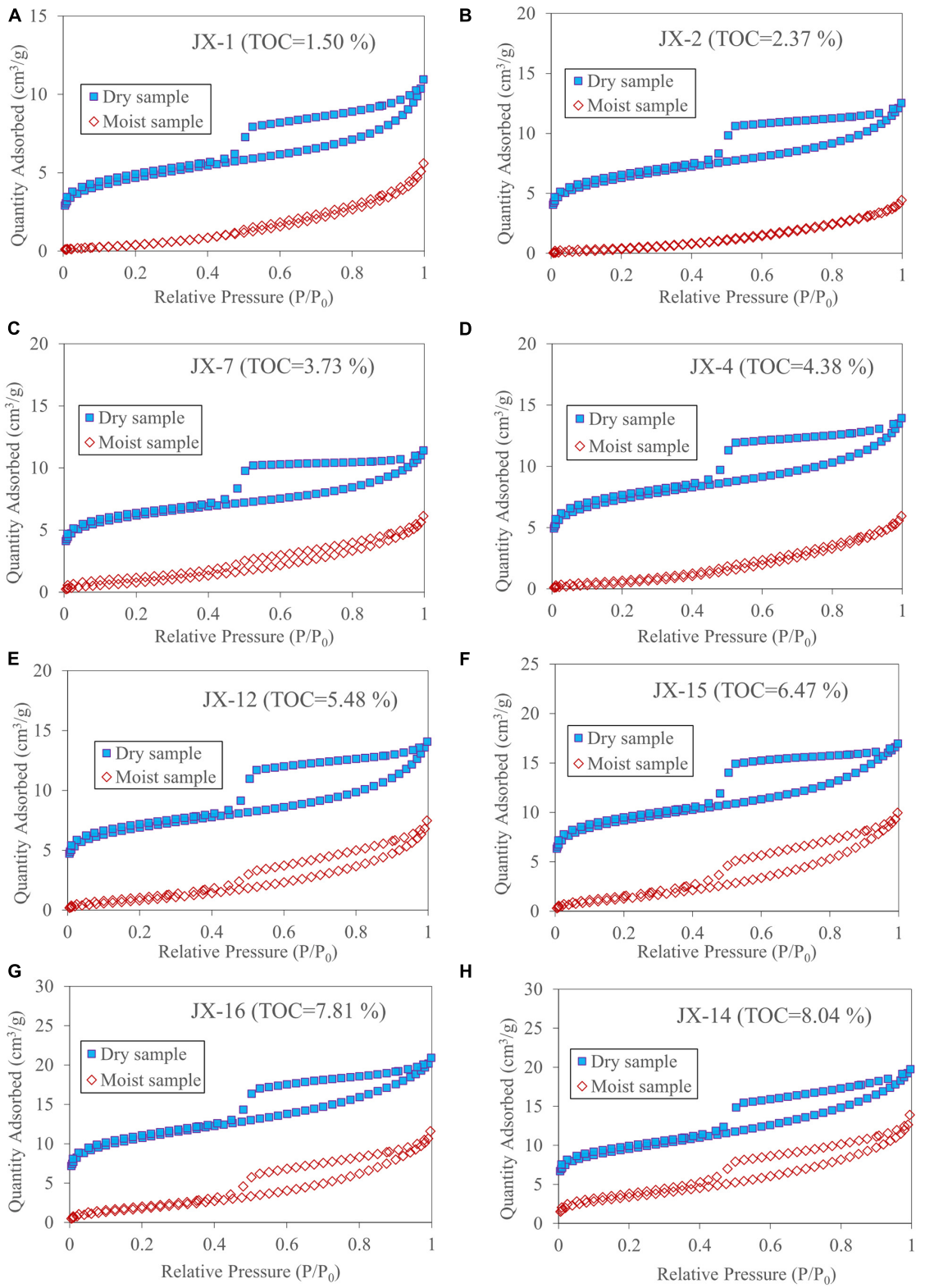

FIGURE 2 | Plots displaying a comparison of the low-pressure N_2 adsorption and desorption isotherms of the selected 8 pairs (moist and dry) shale samples with different TOC contents **(A–H)**. The difference between the moist and dry samples indicates that water influences the N_2 adsorption capacity and pore structure. Besides, the N_2 adsorption quantities of different samples are likely related to their TOC contents, which will be discussed in see section "Controlling Factors of the Shale Pore Structure."

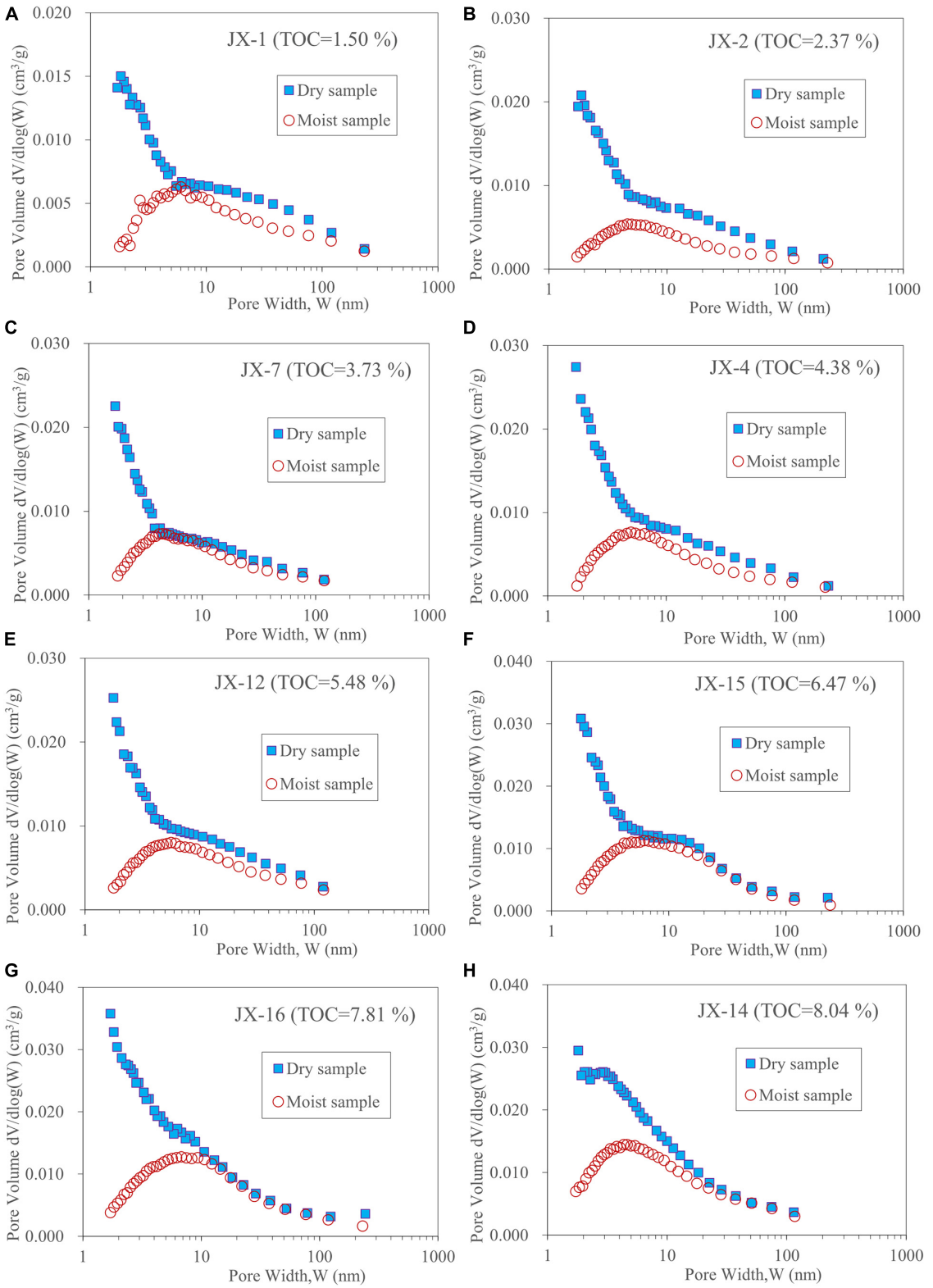

FIGURE 3 | Plots showing the BJH pore-size distributions of the selected 8 pairs (dry and moist) samples based on the N_2 adsorption analysis **(A–H)**. The dry and moist samples have different PSD shapes. Note that water in sample JX-2 **(B)** occupies a broader pore size range compared with other samples shown in **A,C–H**, up to 110 nm, may be due to, in part, its greater pore water content (**Table 2**).

Meanwhile, the shape of hysteretic loop for the dry sample is typically Type B, indicating the fracture-type pore is dominant (Brunauer et al., 1940; De, 1958). However, the hysteresis loop of the moist sample is less developed than that of the dry sample, especially the samples with low TOC contents (such as samples JX-1, JX-2, and JX-4 concomitantly with a higher water content), their hysteresis loops are not notable. It can be seen from the above results that not only the irreducible water in the shales takes up some pore spaces, but it also changes the pore structure characteristics to some extent, especially for the low TOC samples.

The BET surface area (S_{BET}), representative for non-micropores, of the dry sample is 6.16–14.83 m^2/g and averages 10.17 m^2/g. The S_{BET} of the moist sample is obviously lower than that of its corresponding dry sample, and has a range of 2.15–6.66 m^2/g (the average value is about 4.00 m^2/g) (**Table 1**). Compared with the dry sample, the S_{BET} of the moist sample is reduced averagely by 61%.

Figure 3 presents the BJH pore-size distributions (PSD) for the moist and dry samples. For the dry sample, the PSD tends to decrease with increasing pore size, the non-micropores are mainly distributed in the pores <10 nm, and meanwhile, an overall increase in PSD value was observed with increasing TOC. However, for the moist sample, the PSD shows a unimodal peak, and the main peak appears in the pore range of 4–7 nm (**Figure 3**). Compared with the dry sample, the PSD of the moist sample decreases notably in the pores <10 nm. The difference between the dry and moist samples is not significant for the pores >10 nm, indicating the water is mostly distributed in the pores <10 nm. It should be noted that, compared with samples JX1 and JX7, the adsorption quantity and PSD value of sample JX2 are slightly higher under the dry condition and lower under the moist condition, which is likely attributed to its greater clay mineral content (51.60%) (**Table 2**).

TABLE 2 | Data of total S_{BET} and V_{mic}, and calculated organic and inorganic S_{BET} and V_{mic} of the studied samples under dry and moist conditions.

Sample ID	Pore structure parameter	Moist sample	Dry sample	Moist sample		Dry sample	
		Total pore		OM pore	IM pore	OM pore	IM pore
JX-1	BET surface area (m^2/g)	2.15	6.16	1.01	1.14	1.71	4.45
JX-2		2.58	7.94	1.59	0.99	2.70	5.24
JX-3		3.13	8.91	1.83	1.30	3.10	5.81
JX-4		3.53	10.01	2.95	0.58	4.99	5.03
JX-5		3.42	9.79	2.79	0.63	4.73	5.07
JX-6		2.97	9.77	2.54	0.43	4.30	5.47
JX-7		2.93	8.53	2.51	0.42	4.25	4.29
JX-8		3.41	9.07	2.43	0.98	4.11	4.96
JX-9		4.05	9.94	3.01	1.04	5.10	4.83
JX-10		3.50	9.16	2.86	0.64	4.84	4.32
JX-11		4.52	10.26	3.34	1.17	5.66	4.60
JX-12		4.37	9.50	3.69	0.69	6.24	3.26
JX-13		5.01	12.85	4.76	0.26	8.05	4.80
JX-14		6.66	14.04	5.41	1.25	9.16	4.88
JX-15		5.21	11.96	4.35	0.86	7.37	4.59
JX-16		6.53	14.83	5.25	1.28	8.89	5.93
JX-1	Micropore volume (cm^3/g)	0.0039	0.0060	0.0014	0.0026	0.0017	0.0043
JX-2		0.0046	0.0070	0.0021	0.0025	0.0026	0.0044
JX-3		0.0056	0.0076	0.0024	0.0031	0.0030	0.0046
JX-4		0.0065	0.0100	0.0039	0.0026	0.0048	0.0052
JX-5		0.0060	0.0100	0.0037	0.0022	0.0046	0.0055
JX-6		0.0062	0.0092	0.0034	0.0028	0.0042	0.0051
JX-7		0.0064	0.0089	0.0034	0.0031	0.0041	0.0048
JX-8		0.0059	0.0090	0.0032	0.0026	0.0040	0.0050
JX-9		0.0069	0.0095	0.0040	0.0029	0.0049	0.0046
JX-10		0.0065	0.0093	0.0038	0.0026	0.0047	0.0046
JX-11		0.0067	0.0103	0.0045	0.0022	0.0055	0.0048
JX-12		0.0083	0.0112	0.0049	0.0034	0.0060	0.0052
JX-13		0.0083	0.0117	0.0064	0.0019	0.0078	0.0039
JX-14		0.0094	0.0131	0.0072	0.0022	0.0088	0.0042
JX-15		0.0088	0.0125	0.0058	0.0030	0.0071	0.0053
JX-16		0.0099	0.0131	0.0070	0.0028	0.0086	0.0045

Low Pressure CO_2 Adsorption and Pore Distribution

Figure 4 shows the CO_2 adsorption isotherms of the dry and moist samples. The shape of the adsorption isotherms of the dry sample exhibits Type I, which likes that of the moist sample, suggesting both the dry and moist samples present abundant micropores. Furthermore, the CO_2 adsorption quantities of the moist sample are slightly less than those of the corresponding dry sample. Combined with **Figures 2**, **3**, it can be considered that the influence from the irreducible water on micropores is relatively less than that on non-micropores.

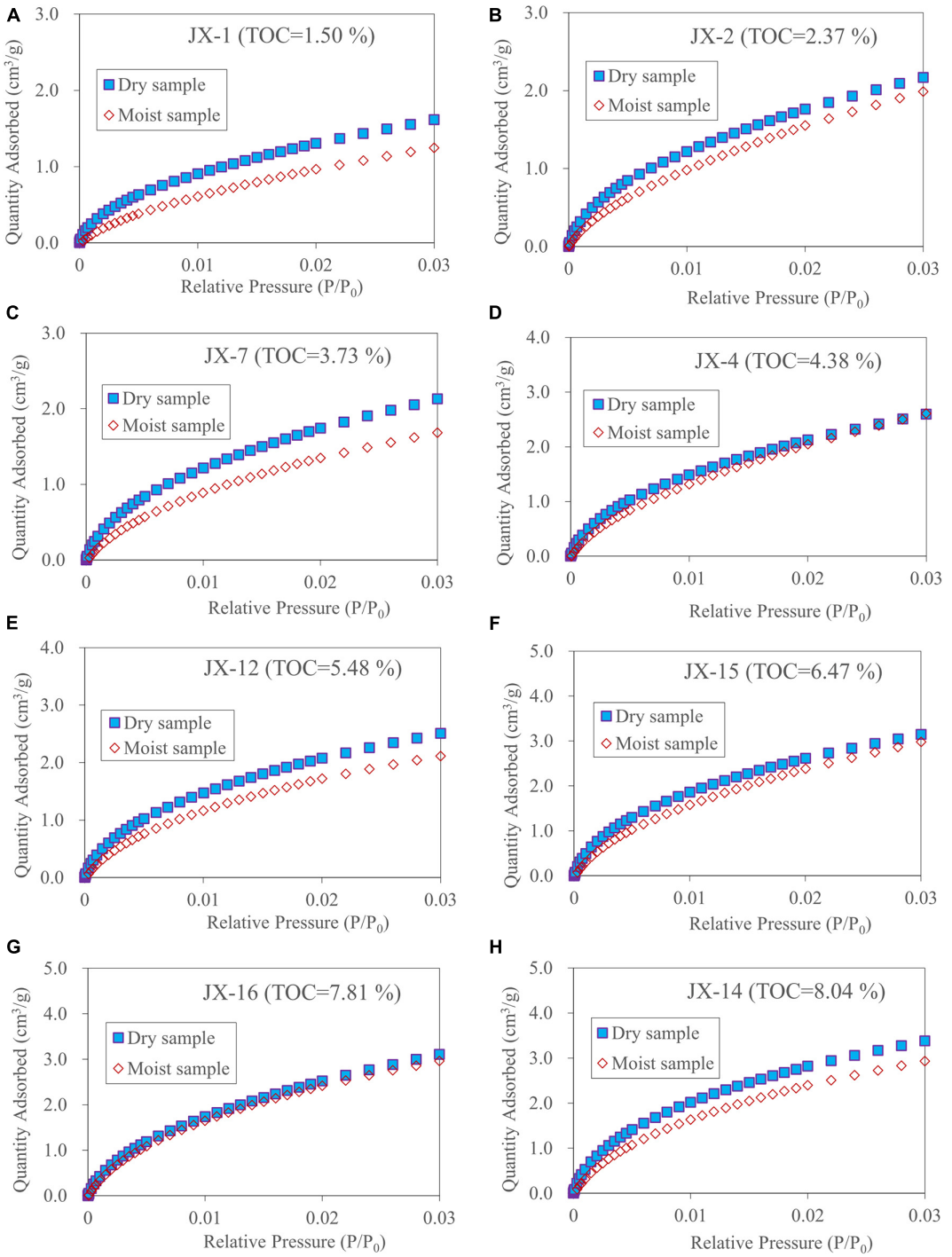

FIGURE 4 | Plots showing the low-pressure CO_2 adsorption isotherms of the selected 8 pairs (dry and moist) samples **(A–H)**. The adsorption isotherm shape and adsorption quantity of the moist sample are close to those of the corresponding dry sample, implying a small effect of irreducible water on micropores.

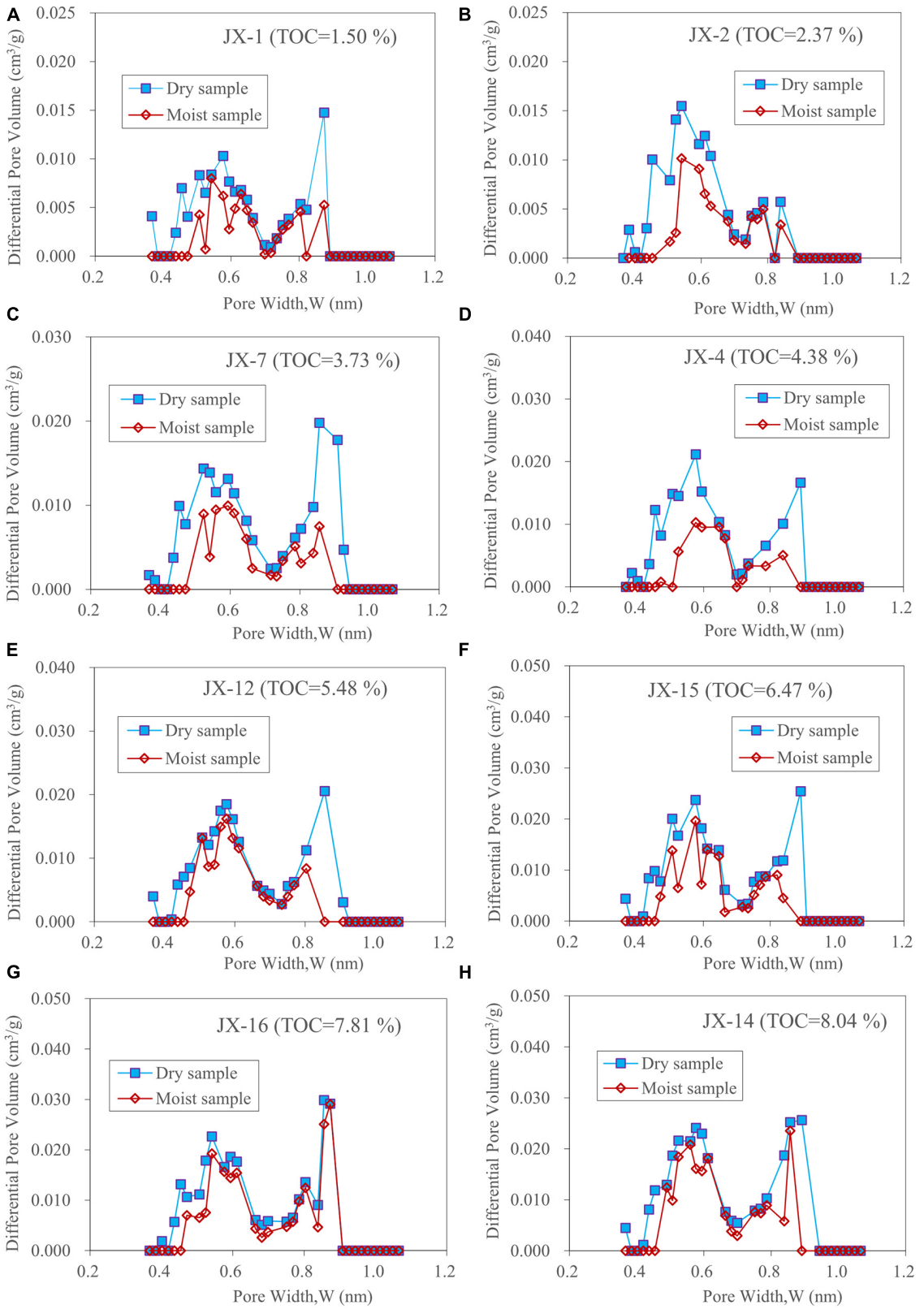

FIGURE 5 | Plots showing the pore-size distribution of the selected 8 pairs (dry and moist) samples based on the CO_2 adsorption analysis **(A–H)**. There is no distinct difference between the dry and moist samples.

The micropore volume (V_{mic}) of the dry sample is 0.0060–0.0131 cm^3/g (an average of 0.0099 cm^3/g), while the moist sample has a V_{mic} of 0.0039–0.0099 cm^3/g (an average of 0.0069 cm^3/g) (**Table 1**). Compared to the dry sample, the V_{mic} of the moist sample cut down about 30% on average, much less than the reduction extent of the S_{BET} (61% on average).

The micropore PSDs of the moist and dry samples were presented in **Figure 5**. It is clear that the dry sample displays a similar PSD to that of the moist sample, and both of them show bimodal characteristics. The main peaks of the PSD values of the dry sample occur at approximately 0.52–0.58 nm and 0.84–0.89 nm, respectively, and those of the moist sample occur at 0.54–0.59 nm and 0.79–0.87 nm, respectively. Moreover, the PSD value of the moist sample differs little from that of the corresponding dry sample, further illustrating that the influence of the irreducible water on micropores is less than that on non-micropores. It should be pointed out that the maximum equilibrium pressure (P/P_0) of the CO_2 adsorption experiment in the present study was about 0.03 (1 bar), which is significant lower than the CO_2 saturation pressure at 273 K (34.5 bar), hence the effective micropore range characterized by our CO_2 adsorption experiment is only 0.36–0.93 nm, while the larger micropores (0.93–2.00 nm) were not detected.

Controlling Factors of the Shale Pore Structure

Figure 6 displays the relationships of TOC and clay mineral contents with the S_{BET} (**Figures 6A,B**) and V_{mic} (**Figures 6C,D**). To avoid the impact of clay minerals on the pore structure parameters being masked by TOC, the S_{BET}, and V_{mic} were normalized to per unit TOC (1%), so they can directly reflect the contribution of clay minerals to the S_{BET} and V_{mic}. For the dry sample, the S_{BET} is positively linearly correlated with TOC, having a correlation coefficient(R^2)of 0.92 (**Figure 6A**), and a linear relationship also exists between the S_{BET} and the clay mineral (R^2 = 0.47) (**Figure 6B**). These results imply the S_{BET} of the dry sample is controlled by both TOC and clay minerals, and the former is the main controlling factor, which is because the clay minerals in the studied samples consist of chlorite and illite (Sun et al., 2020) with low specific surface areas (Gasparik et al., 2012; Ji et al., 2012; Liu et al., 2018).

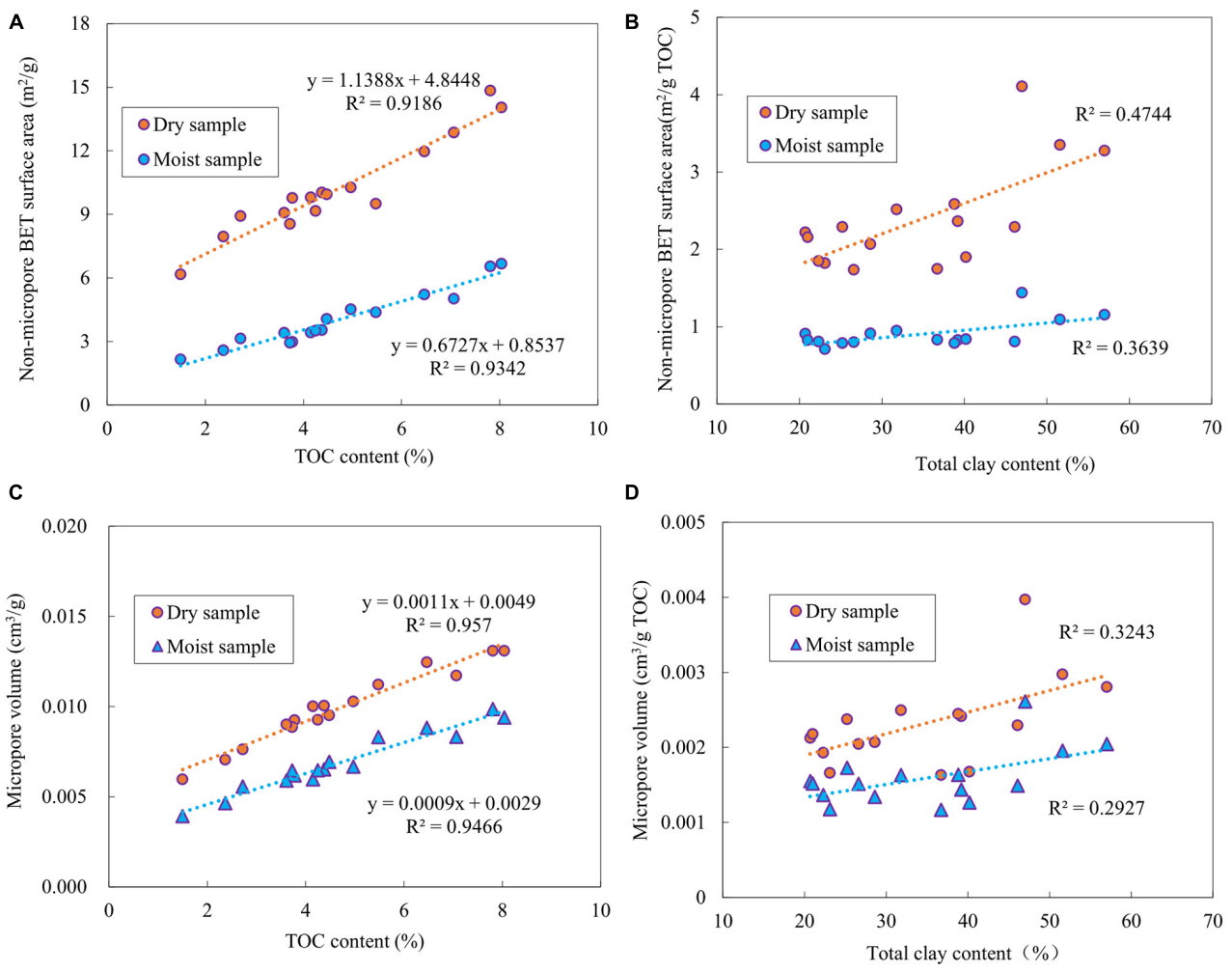

FIGURE 6 | The correlations of S_{BET} **(A,B)** and V_{mic} **(C,D)** with TOC and clay minerals.

For the moist sample, the S_{BET} still has an obvious positive linear correlation with TOC (R^2 = 0.93) (**Figure 6A**), however, its correlation with clay minerals decreases (the R^2 reduces from 0.47 to 0.36) (**Figure 6B**). Therefore, a conclusion can be made that the irreducible water shows a more obvious influence on the non-micropores of clay minerals compared with that of organic matter.

The V_{mic} of the dry sample shows a notable positive linear correlation with TOC (R^2 = 0.96) (**Figure 6C**), and a weak positive linear correlation with clay minerals (R^2 = 0.32) (**Figure 6D**). For the moist sample, the V_{mic} is still apparently correlated to TOC (R^2 = 0.95) (**Figure 6C**), while the weak linear relationship seems exist between the V_{mic} and clay minerals, but having a lower R^2 value (0.29) compared to

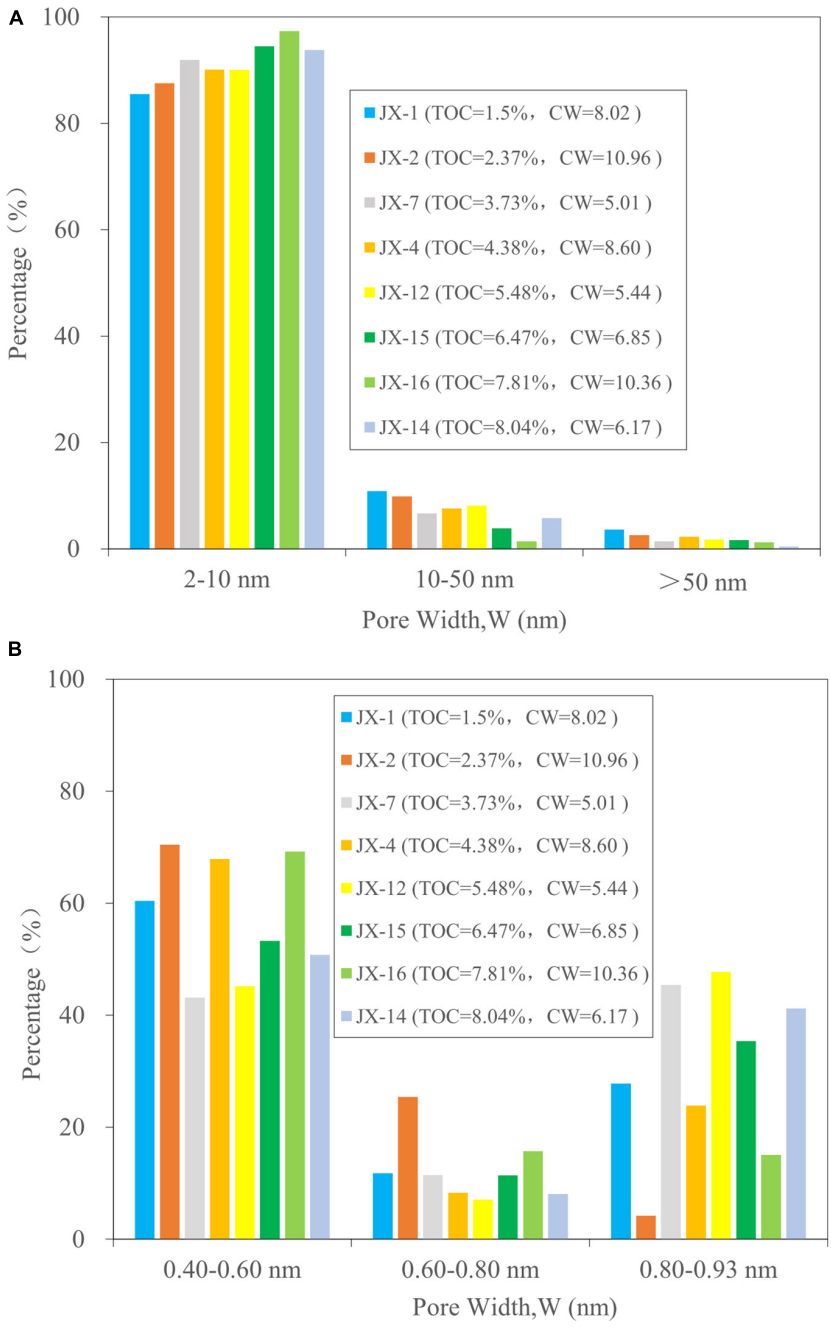

FIGURE 7 | Percentages occupied by irreducible water in the non-micropores **(A)** and micropores **(B)** for the selected 8 samples. It should be pointed out that pores smaller than 0.40 nm were not counted since the diameter of H_2O molecules is approximately 0.40 nm, and the percentages occupied by water in the pores of 0.93–2.00 nm were not observed since the effective micropore range is only 0.36–0.93 nm in the present study.

the dry sample (**Figure 6D**). Combined with **Figure 6B**, it is clear that the effect of the irreducible water on micropores is less significant than that on non-micropores. This is because clay minerals have a greater contribution to mesopores and macropores than that to the micropores (Chalmers and Bustin, 2008; Bakshi et al., 2017, 2018).

Occurrence of Irreducible Water in Shale Nanopores

Occurrence of Pore Water in Different Size Nanopores

Occurrence of the irreducible water in different size nanopores can be reflected by their volumes occupied by the water in different pore sizes relative to the total pore volume occupied by the water. For a specific shale sample, these volumes occupied by the water can be largely calculated by the difference between its dry and moist conditions. As seen from the results of the representative samples in **Figure 7**, in the range of non-micropores, the percentages occupied by the water decrease with increasing pore size. The water occurs mainly in the pores of 2–10 nm, and the occupation percentage varies from 85.50 to 97.34%. This is followed by the pores of 10–50 nm, with an occupation percentage range of 1.44–10.88%, while the percentage occupied by the water in macropores (>50 nm) is the lowest, which is 0.42–3.62% (**Figure 7A**). In the micropore range, the water occurs mostly in the pores of 0.40–0.60 nm and 0.80–0.93 nm, with average percentages of 57.54 and 30.07%, respectively. The occupied volume in pores between 0.60 and 0.80 nm is the least, with an average percentage of about 12.39% (**Figure 7B**). According to the above results, the irreducible water distributes mainly in mesopores of <10 nm and micropores of 0.40–0.60 nm and 0.80–0.93 nm.

Occurrence of Irreducible Water in OM and IM Nanopores

It is conventionally believed that inorganic matter (such as clay minerals) pores are hydrophilic and the organic pores are hydrophobic. However, a few recent papers document that water occurs widely in organic pores especially in high and over mature shales (Cheng et al., 2017, 2018). There

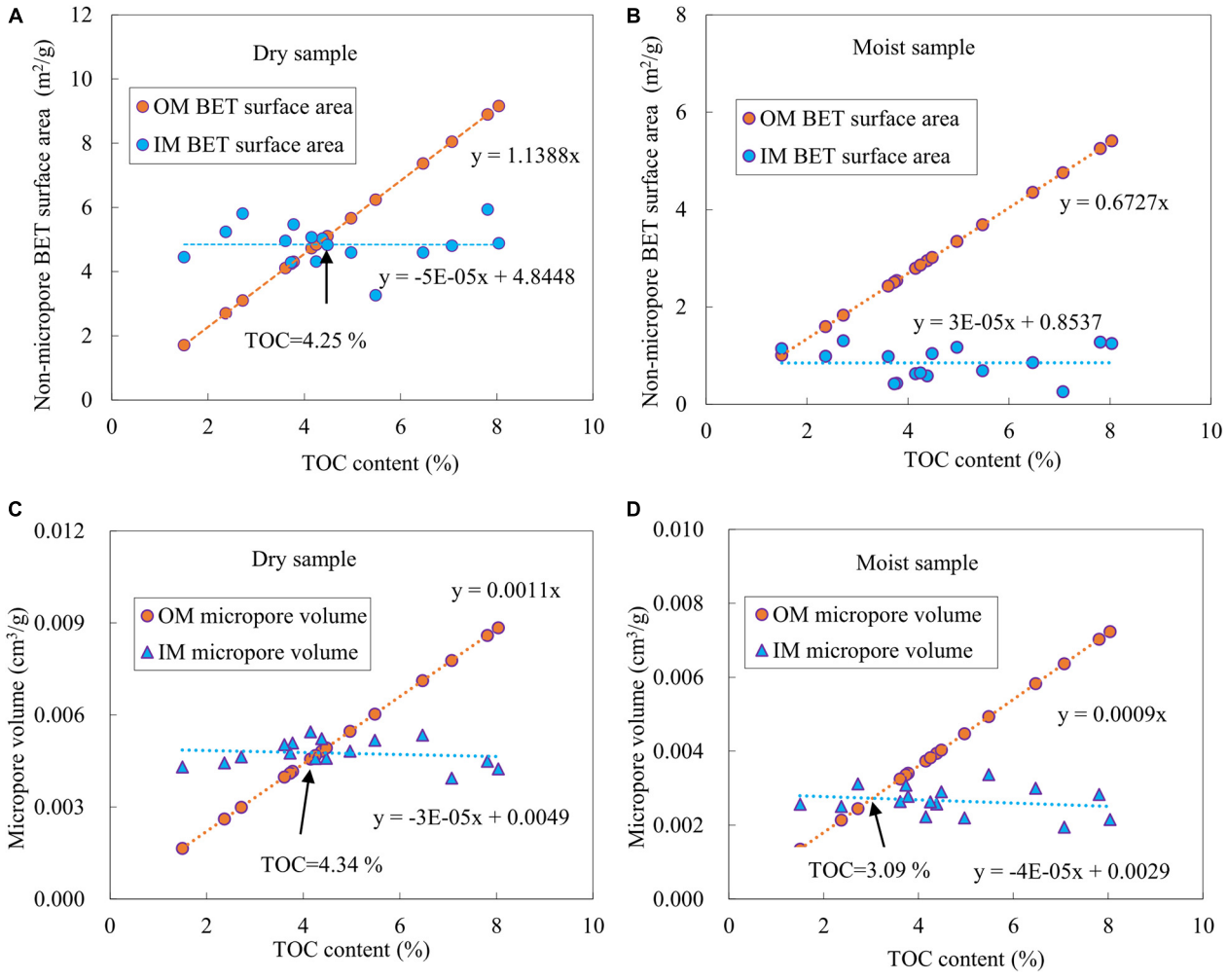

FIGURE 8 | The relationships of TOC with S_{BET-OM}, S_{BET-IM} **(A,B)**, and V_{mic-OM}, V_{mic-IM} **(C,D)** for the dry and moist samples. See details in text.

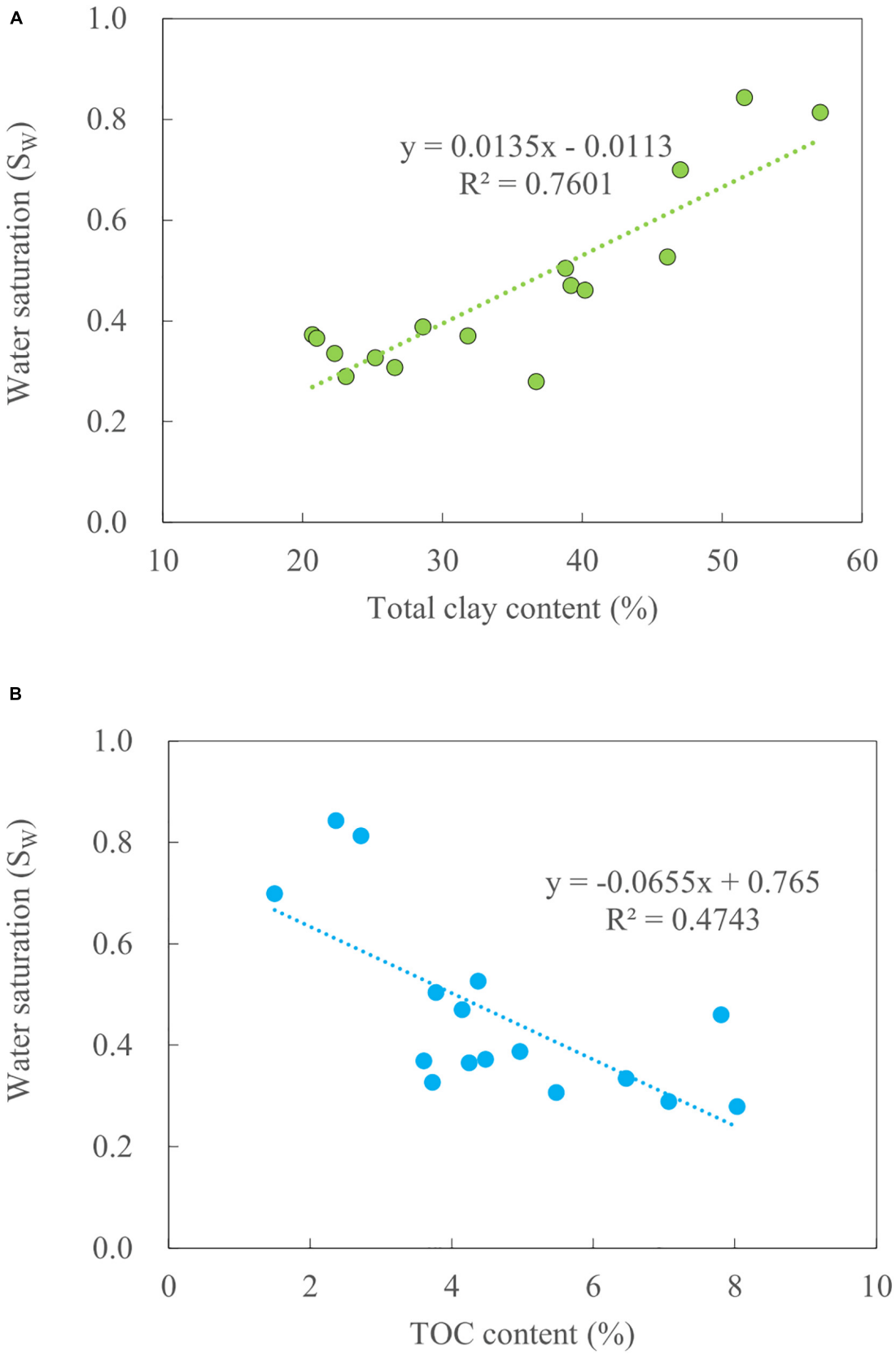

FIGURE 9 | Relationships of S_W with total clay mineral **(A)** and TOC contents **(B)**. See details in text.

are mainly two understandings on the mechanism of the hydrophilicity of organic pore. One is that some organic pore surfaces contain hydrophilic adsorption sites, such as oxygen-containing groups (Bahadur et al., 2017), water molecules can be adsorbed to the organic pore surfaces by forming hydrogen bonds with oxygen-containing groups. Moreover, even if the organic pore contains no containing-oxygen groups, it is inherently hydrophilic (Kozbial et al., 2014; Wei and Jia, 2015). Therefore, water can occupy both in shale inorganic and organic pores.

It is difficult to determine the OM and IM pores of shale samples precisely (Löhr et al., 2015). The means based on the linear positive relationship between TOC and total porosity for a set of shale samples is commonly adopted at present. According to this method, the OM porosity of a shale sample is the product of its TOC and the regressed line slope, and the difference between its total porosity and OM porosity is considered to be the IM porosity (Zhang et al., 2012; Tian et al., 2013, 2015; Hu et al., 2017; Sun et al., 2020). In the present study, the S_{BET} and V_{mic} of both the moist and dry samples exhibit strong positive linear correlations with TOC (R^2 values of 0.91–0.95) (**Figures 6A,C**). Therefore, the above linear regression method can be also applied to estimate the OM and IM pore structure parameters (S_{BET} and V_{mic}) of the studied samples, as reported by Cheng et al. (2018). The OM S_{BET} of a shale sample is the product of its TOC and the regressed line slope (**Figure 6A**), and the difference between its total S_{BET} and OM S_{BET} is considered to be the IM S_{BET}; the estimation of OM, IM V_{mic} is based on the same method.

The determined results indicate that the S_{BET-OM} (BET surface area of OM) and S_{BET-IM} (BET surface area of IM) values of the dry sample are 1.71–9.16 and 3.26–5.93 m^2/g, respectively (**Table 1**), and that the S_{BET-OM} is greater than the S_{BET-IM} for the samples with TOC contents >4.25% (**Figure 8A**). However, for the moist sample, the S_{BET-OM} and S_{BET-IM} values are 1.01–5.41 and 0.26–1.30 m^2/g, respectively (**Table 1**), and the S_{BET-OM} is greater than the S_{BET-IM} for all studied samples (**Figure 8B**).

The V_{mic-OM} (OM micropore volume) and V_{mic-IM} (IM micropore volume) values of the dry sample are 0.0017–0.0088 and 0.0039–0.0055 cm^3/g, respectively, and those of the moist sample are 0.0014–0.0072 and 0.0019–0.0034 cm^3/g, respectively (**Table 1**). Moreover, the V_{mic-OM} is greater than the V_{mic-IM} for the dry samples with TOC contents >4.34% (**Figure 8C**) and for the moist samples with TOC contents >3.09% (**Figure 8D**).

It was supposed that the difference of pore structure parameters between the moist and dry samples could present the space taken by the irreducible water. A further calculation based on the data in **Table 1** reports that the water occupies 82% of the S_{BET-IM} and 41% of the S_{BET-OM}, and 44% of the V_{mic-IM} and 18% of the V_{mic-OM} for the studied shale samples. Therefore, it is believed the irreducible water occurs preferentially in the IM pores, occupying a greater part of their non-micropore surface areas, and near a half of their micropore volumes, but its influence on the OM pores is limited, and most of the OM pores can still provide spaces for the storage of shale gas.

Gas-Bearing Property and Its Controlling Factors

Control of TOC on Gas-Bearing Property

The water saturation (S_W) of the studied shale samples varies greatly, ranging from 27.71 to 84.28%, with an average of 45.83% (**Table 3**). It is close to that of the Longmaxi shales from the wells Shao101 and YQ1 (>60%) outside the Sichuan Basin (Liu and Wang, 2013; Fang et al., 2014), and greater than that of the Longmaxi shales in the Sichuan Basin (10–45%) (Liu and Wang, 2013; Fang et al., 2014; Wei and Wei, 2014) and the gas shales in North America (10–35%) (Boyer et al., 2006; Bowker, 2007;

TABLE 3 | Calculated data of water saturation, and absorbed and free gas contents of the studied shale samples.

Sample ID	Depth (m)	TOC (%)	Water Saturation (%)	Gas content (m^3/t)			Percentage of adsorbed gas (%)	Percentage of free gas (%)
				Free gas	Adsorbed gas	Total gas [a]		
JX-1	362.61	1.50	69.88	0.13	0.75	0.88	85.63	14.37
JX-2	366.90	2.37	84.28	0.08	1.09	1.17	93.45	6.55
JX-3	370.04	2.72	81.28	0.11	1.10	1.21	91.22	8.78
JX-4	375.06	4.38	52.65	0.29	1.15	1.44	79.72	20.28
JX-5	376.78	4.15	46.92	0.35	1.26	1.61	78.12	21.88
JX-6	377.51	3.78	50.36	0.32	0.78	1.10	71.20	28.80
JX-7	381.70	3.73	32.62	0.40	0.77	1.17	66.06	33.94
JX-8	383.56	3.61	36.90	0.41	0.93	1.34	69.45	30.55
JX-9	385.26	4.48	37.17	0.36	0.90	1.26	71.72	28.28
JX-10	387.52	4.25	36.43	0.35	0.93	1.28	72.31	27.69
JX-11	388.89	4.97	38.69	0.40	0.88	1.28	68.56	31.44
JX-12	390.48	5.48	30.65	0.48	1.91	2.39	79.78	20.22
JX-13	391.92	7.07	28.70	0.54	1.52	2.06	73.75	26.25
JX-14	392.36	8.04	27.71	0.63	2.09	2.72	76.76	23.24
JX-15	393.03	6.47	33.28	0.54	2.17	2.71	80.10	19.90
JX-16	394.01	7.81	45.77	0.48	2.56	3.04	84.12	15.88

[a]: *Data cited from Sun et al. (2020).*

Cipolla et al., 2010; Wang, 2012). As illustrated in **Figure 9**, the S_W is positively related to the total clay minerals (R^2 = 0.76, **Figure 9A**), but presents a negative linear relationship to some extent with TOC (R^2 = 0.47, **Figure 9B**). This implies the irreducible water not only mostly occurs, but also has a greater saturation in the pores of clay minerals.

The calculated free gas (Q_{free}) and adsorbed gas (Q_{ads}) of the studied samples are presented in **Table 3**. The Q_{free} is 0.08–0.63 m^3/t and averages 0.37 m^3/t, while the Q_{ads} is 0.75–2.56 m^3/t and averages 1.30 m^3/t, accounting for 66.06–93.45% of the total gas (77.62% on average). Pan et al. (2016) reported a GIP model based on a Longmaxi shale (TOC = 3.98%) from the Pengshui Block, South China. According to their GIP model, at the depth of 400 m, the Q_{ads} is about 88% of the GIP content without taking into account the influence of the pore water. For the well XK2 in the present study, the adsorbed gas percentage of the shale samples with TOC≈4% is in the range of 70–80%, indicating the irreducible water should reduce the Q_{ads} to some extent.

Figure 10 presents the positive linear relationships of TOC with the Q_{free} and Q_{ads} for the studied samples, with R^2 values of 0.67 and 0.80, respectively. The correlation coefficient between the TOC and Q_{ads} is significantly lower than that between the TOC and methane adsorption capacity reported by Pan et al. (2016) on the basis of dry Longmaxi samples (R^2 : 0.96–0.97), and similar to that proposed by Chalmers and Bustin (2008) based on the moisture-equilibrated shale samples (R^2 = 0.67). Therefore, compared with the dry shale samples, not only the actual adsorption capacity of the moist sample is reduced, but its correlation with TOC is also decreased, and the high-pressure CH_4 adsorption experiment results conducted on dry shale samples can not be directly applied to the geological adsorption gas evaluation.

Based on the linear regression equations presented in **Figure 10**, the Q_{ads} and Q_{free} in OM and IM pores for the studied samples were also estimated by a similar method discussed in section "Occurrence of Irreducible Water in OM and IM

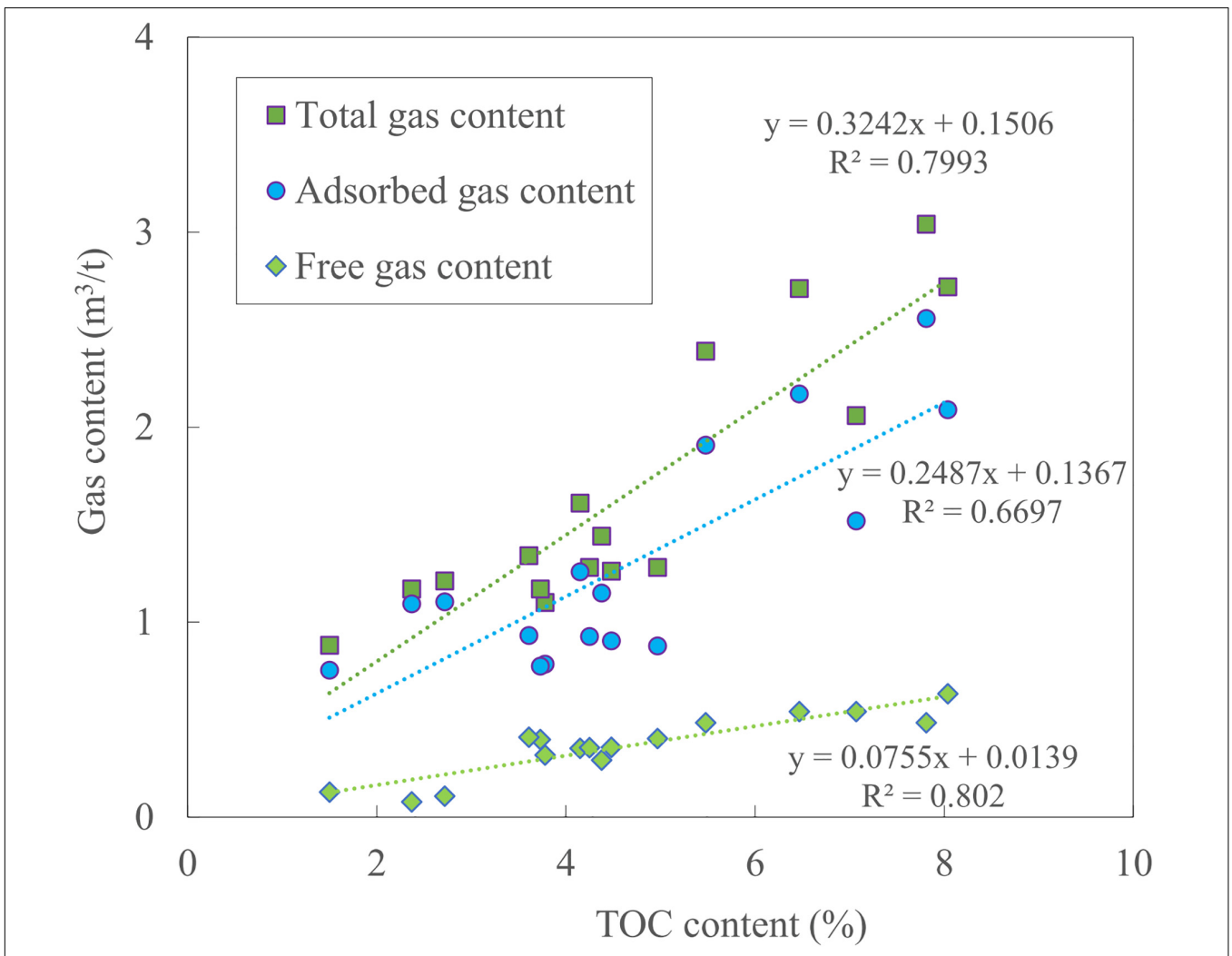

FIGURE 10 | Correlations of TOC with free, adsorbed, and total gasses for the studied shale samples. Their positive correlations indicate that TOC directly controls the gas-bearing property, so the adsorbed and free gas contents in the OM and IM pores could be determined from their linear regression equations.

Nanopores". The calculated Q_{ads} and Q_{free} in OM pores are 1.16 and 0.35 m^3/t on averages, respectively, accounting for 89% of the total absorbed gas and 95% of the total free gas, and those in IM pores are 0.14 and 0.02 m^3/t on averages, respectively, accounting for 11% of the total absorbed gas and 5% of the total free gas. From those results, a conclusion could be draw that the shale gas stored mostly in OM pores, and IM pores contain a little gas due to the effect of irreducible water.

Relationship Between Irreducible Water and Gas-Bearing Property

Figure 11 presents the relationships of the GBP (presented by Q_{total}, Q_{ads}, and Q_{free}) with the water content (**Figures 11A,B**) and water saturation (S_W) (**Figures 11C,D**). The Q_{ads} shows a rapid drop and then a slow decrease (**Figure 11A**) with increasing the water content. Since the shale gas of the studied samples is mostly in the adsorbed state, the trend of the Q_{total} follows that of the Q_{ads} (**Figure 11B**). In **Figure 11A**, the data of Lower Cretaceous shales from British Columbia, Canada reported by Ross and Bustin (2009) were included, and the two sets of data seem keeping the same trend with increasing water content.

The relationships of the S_W with the Q_{total}, Q_{ads}, and Q_{free} follow similar trends as described above. As the S_W is less than 40%, the Q_{ads} and Q_{tota} decrease rapidly with increasing S_W (**Figures 11C,D**), but these trends tend to slow with further increasing S_W (**Figures 11C,D**). This result is in agreement with that of the Longmaxi shale in the Weiyuan-Changning Block, Sichuan Basin reported by Hu et al. (2018). They revealed that the Q_{ads} declined significantly in the S_W range of <30%, while it decreased slowly when the S_W increased from 30 to 50%.

The influences of the irreducible water on the GBP can be explained by its occurrence characteristics in different nanopores. According to our results, the irreducible water occurs mostly in non-micropores, especially the non-micropores of clay minerals, with a great reduction of their non-micropore surface areas. Although OM pores also contain a small amount of irreducible water, the reductions of their non-micropore surface areas and micropore volumes are limited due to their hydrophobic nature. Therefore, the irreducible water mainly affects the adsorption capacity of IM pores, and OM pores contribute mostly to the shale adsorption capacity. In conditions of low S_W, the water preferentially occupies the pores in clay minerals, significantly decreases their adsorption capacities, causing the adsorbed gas decrease rapidly with increasing the water content or S_W. With the further increase of S_W, the reduction of adsorption capacity is still mainly from clay minerals even when the S_W reaches a high level, while the OM pores still have a certain adsorption capacity. This is why the absorbed gas content decreases slowly

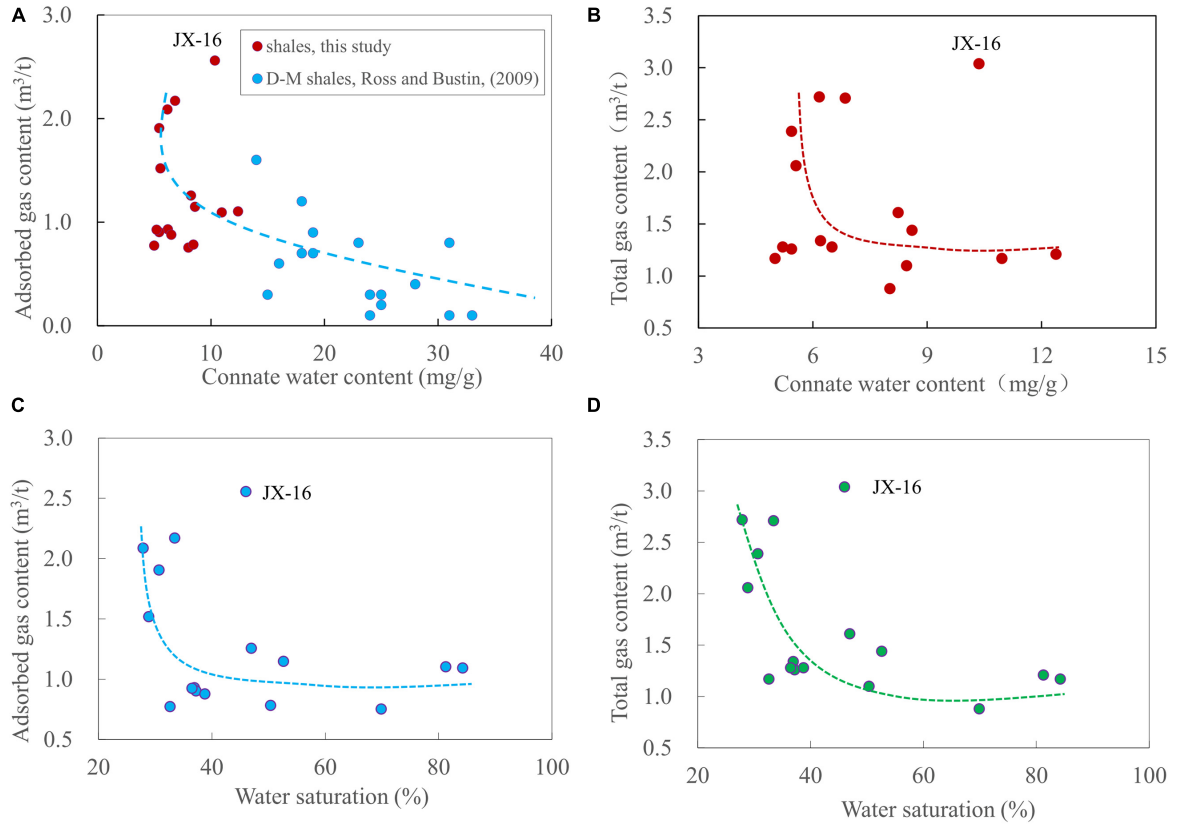

FIGURE 11 | Plots showing the relationships of irreducible water contents with the Q_{ads} **(A)** and Q_{total} **(B)**, and the correlations of the S_W with the Q_{ads} **(C)** and Q_{total} **(D)**. The D-M shale data were measured at 30°C (Ross and Bustin, 2009). It should be noted that, since the sample JX-16 is away from the trend of the regression line, the regression line have not included the data of this sample.

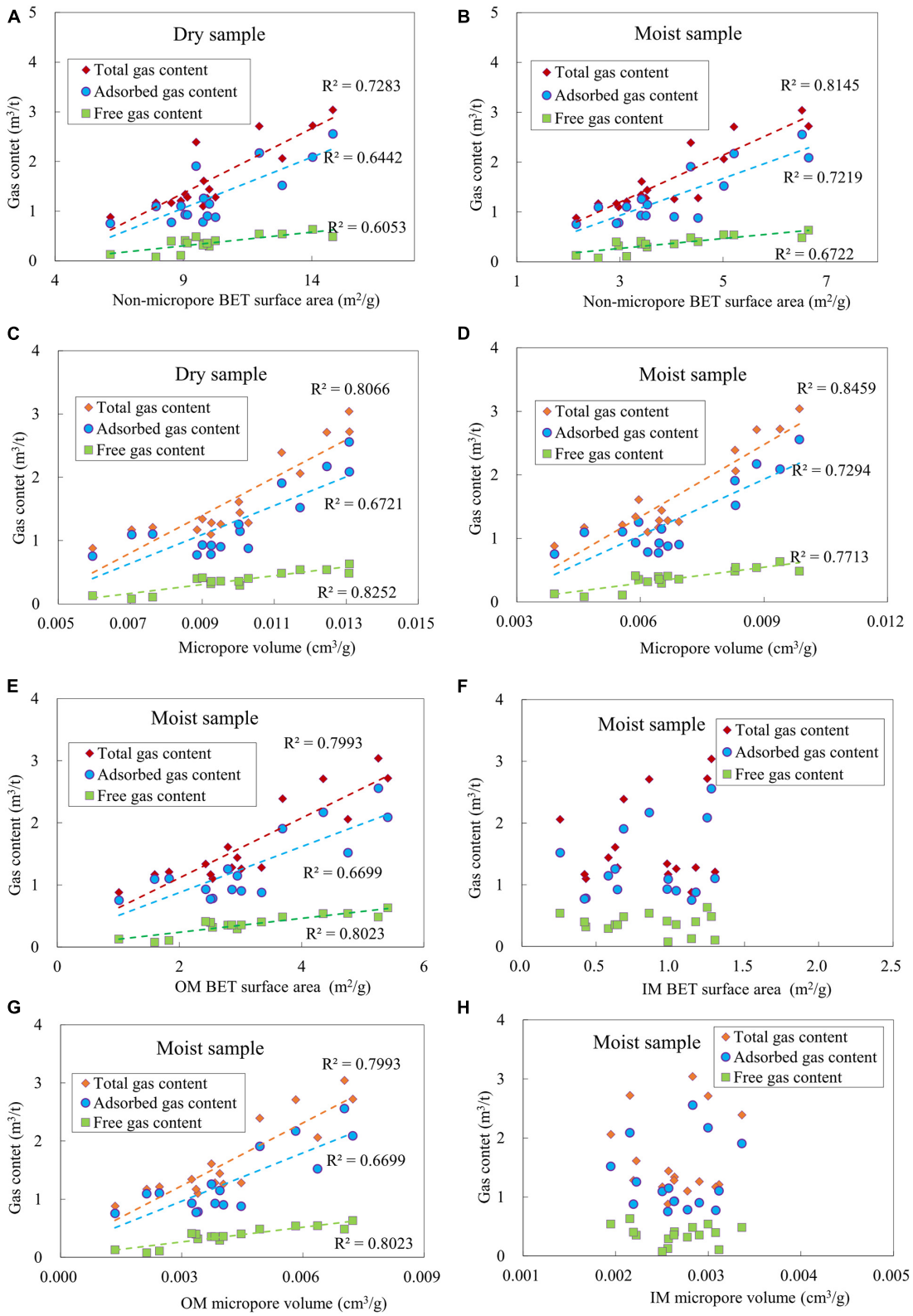

FIGURE 12 | Plots showing the correlations of the contents of absorbed, free and total gasses with the BET surface areas **(A,B)** and micropore volumes **(C,D)** for the studied shale samples, and the relationships of the contents of absorbed, free and total gasses with the OM, IM BET surface areas **(E,F)** and OM, IM micropore volumes **(G,H)** for the moist shale samples. **(A–D)** their correlations of the moist sample are obviously better than those of the dry sample; **(E–H)** the gas-bearing property shows positively relationships with the OM pore structure parameters, while displays no correlations with the IM pore structure parameters.

with further increasing water content or S_W as it exceeds a certain amount.

Figures 12A–D displays the correlations between the pore structure parameters (S_{BET} and V_{mic}) and GBP (Q_{total}, Q_{ads}, and Q_{free}) for both the moist and dry samples. It is clear that their correlations are better for the moist sample than those for the dry sample. **Figures 12E–H** further represents the relationships of the Q_{total}, Q_{ads}, and Q_{free} with either OM or IM pore structure parameters for the moist sample. They display obvious positive linear correlations with the OM pores, but reveal unclear correlations with the IM pores. Chalmers and Bustin (2008) made an explanation for a high CH_4 adsorption capacity of the moisture-equilibrated shale samples. They claimed gas and water took different sorption sites in shales. The present study results further demonstrate that the OM pores provide the most sorption sites for shale gas and control the Q_{ads}, affecting the GBP.

CONCLUSION

The pore structure, irreducible water occurrence characteristics, gas-bearing property, and their relationships of the shallow Longmaxi shales from the well XK2 were investigated, and the main conclusions are as follows:

- The micropore, mesopore, and macropore of the dry and moist samples are all well developed. Compared with the dry sample, the non-micropore BET surface area and micropore volume of the moist sample are reduced by 61 and 30% on averages, respectively.
- The irreducible water occurs mainly in IM pores, especially smaller mesopores (2–10 nm). The water occupies averagely 82 and 41% of the inorganic and organic non-micropore BET surface areas, respectively, and 44 and 18% of the inorganic and organic micropore volumes, respectively.
- The irreducible water significantly reduces the adsorbed gas content in IM pores, but its influence on OM pores is limited, and the OM pores store approximately 89% of the adsorbed gas and 95% of the free gas.

DATA AVAILABILITY STATEMENT

The original contributions presented in the study are included in the article/supplementary material, further inquiries can be directed to the corresponding author.

AUTHOR CONTRIBUTIONS

JS conducted the experimental work, analyzed the data, and wrote the manuscript. XMX designed the study and reviewed the manuscript. QW conducted the experimental work. PC analyzed the data. HT reviewed the manuscript. All authors contributed to the article and approved the submitted version.

FUNDING

This study was jointly supported by the National Natural Science Foundation of China (U1810201, U19B6003-03, 4203000087, and 41925014), and Natural Science Foundation of Guangdong Province (2016A030310119).

ACKNOWLEDGMENTS

Dr. Li Guanfang from Institute of Geology and Geophysics, Chinese Academy of Sciences, is thanked for helping us to collect the shale samples.

REFERENCES

Aringhieri, R. (2004). Nanoporosity characteristics of some natural clay minerals and soils. *Clay. Miner.* 52, 700–704. doi: 10.1346/CCMN.2004.0520604

Bahadur, J., Contescu, C. I., Rai, D. K., Gallego, N. C., and Melnichenko, Y. B. (2017). Clustering of water molecules in ultra-microporous carbon: in-situ small-angle neutron scattering. *Carbon* 111, 681–688. doi: 10.1016/j.carbon.2016.10.040

Bai, J. J., Kang, Y. L., Chen, M. J., Chen, Z. X., You, L. J., Li, X. C., et al. (2020). Impact of surface chemistry and pore structure on water vapor adsorption behavior in gas shale. *Chem. Eng. J.* 402:126238. doi: 10.1016/j.cej.2020.126238

Bakshi, T., Prusty, B. K., Pathak, K., Nayak, B. R., Mani, D., and Pal, S. K. (2017). Source rock characteristics and pore characterization of Indian shale. *J. Nat. Gas Sci. Eng.* 45, 761–770. doi: 10.1016/j.jngse.2017.06.010

Bakshi, T., Prusty, B. K., Pathak, K., and Pal, S. K. (2018). Pore characteristics of Damodar valley shale and their effect on gas storage potential. *J. Nat. Gas Sci. Eng.* 162, 725–735. doi: 10.1016/j.petrol.2017.10.091

Barrett, E. P., Joyner, L. G., and Halenda, P. P. (1951). The determination of pore volume and area distribution in porous substances. I: computations from nitrogen isotherms. *J. Am. Chem. Soc.* 73, 373–380. doi: 10.1021/ja01145a126

Bhowrnik, S., and Dutta, P. (2019). A study on the effect of gas shale composition and pore structure on methane sorption. *J. Nat. Gas Sci. Eng.* 62, 144–156. doi: 10.1016/j.jngse.2018.12.009

Bowker, K. A. (2007). Barnett shale gas production, fort worth basin: issues and discussion. *AAPG Bull.* 91, 523–533. doi: 10.1306/06190606018

Boyer, C., Kieschnick, J., Suarez, R. R., Lewis, R. E., and Waters, G. (2006). Producing gas from its source. *Oilfield Rev.* 18, 36–49.

Brunauer, S., Deming, L. S., Deming, W. E., and Teller, E. (1938). Adsorption of gases inmultimolecular layers. *J. Am. Chem. Soc.* 60, 309–319.

Brunauer, S., Deming, L. S., Deming, W. E., and Teller, E. (1940). On a theory of the van der waals adsorption of gases. *J. Am. Chem. Soc.* 62, 1723–1732. doi: 10.1021/ja01864a025

Bustin, R. M., Bustin, A., Chalmers, D. R. G., Murthy, V., Laxmi, C., and Cui, X. (2008). *Shale Gas Opportunities and Challenges*. San Antonio, TX: AAPG Annual Convention.

Chalmers, G. R. L., and Bustin, R. M. (2007). The organic matter distribution and methane capacity of the lower cretaceous strata of Northeastern British Columbia. *Int. J. Coal Geol.* 70, 223–239. doi: 10.1016/j.coal.2006.05.001

Chalmers, G. R. L., and Bustin, R. M. (2008). Lower Cretaceous gas shales in northeastern British Columbia, part I: geological controls on methane adsorption capacity. *Bull. Can. Pet. Geol.* 56, 1–21. doi: 10.2113/gscpgbull.56.1.1

Chareonsuppanimit, P., Mohammad, S. A., Robinson, R. L., and Gasem, K. A. M. (2012). High-pressure adsorption of gases on shales: measurements and modeling. *Int. J. Coal Geol.* 95, 34–46. doi: 10.1016/j.coal.2012.02.005

Charriere, D., and Philippe, B. P. (2010). Water sorption on coals. *J. Colloid. Interface. Sci.* 344, 460–467. doi: 10.1016/j.jcis.2009.11.064

Chen, S. B., Han, Y. F., Fu, C. Q., Zhang, H., Zhu, Y. M., and Zuo, Z. X. (2016). Micro and nano-size pores of clay minerals in shale reservoirs: implication for

the accumulation of shale gas. *Sedim. Geol.* 342, 180–190. doi: 10.1016/j.sedgeo.2016.06.022

Chen, S. B., Zuo, Z. X., Moore, T. A., Han, Y. F., and Uwamahoro, C. (2018). Nanoscale pore changes in a marine shale: a case study using pyrolysis experiments and nitrogen adsorption. *Energy Fuels* 32, 9020–9032. doi: 10.1021/acs.energyfuels.8b01405

Cheng, P., Tian, H., Xiao, X. M., Gai, H. F., Li, T. F., and Wang, X. (2017). Water distribution in overmature organic-rich shales: Implications from water adsorption experiments. *Energy Fuels* 31, 13120–13132. doi: 10.1021/acs.energyfuels.7b01531

Cheng, P., Xiao, X. M., Tian, H., and Wang, X. (2018). Water content and equilibrium saturation and their influencing factors of the lower paleozoic overmature organic-rich shales in the upper yangtze region of Southern China. *Energy Fuels* 32, 11452–11466. doi: 10.1021/acs.energyfuels.8b03011

Cipolla, C. L., Lolon, E. P., Erdle, J. C., and Rubin, B. (2010). Reservoir Modeling in Shale-Gas Reservoirs. *Paper Presented at the SPE Eastern Regional Meeting*. SPE-125530-MS, Charleston, WV, doi: 10.2118/125530-MS

Clarkson, C. R., and Bustin, R. M. (1999). The effect of pore structure and gaspressure upon the transport properties of coal: a laboratory andmodeling study 1: isotherms and pore volume distributions. *Fuel* 78, 1333–1344. doi: 10.1016/S0016-2361(99)00056-3

Curtis, J. B. (2002). Fractured shale-gas systems. *AAPG Bull.* 86, 1921–1938. doi: 10.1306/61EEDDBE-173E-11D7-8645000102C1865D

Curtis, M. E., Ambrose, R. J., Sondergeld, C. H., and Rai, C. S. (2010). "Structural characterization of gas shales on the micro-and nano-scales," in *Proceedings of the Canadian Unconventional Resources and International Petroleum Conference*, Calgary, ALB, 19–21. doi: 10.2118/137693-MS

Curtis, M. E., Ambrose, R. J., Sondergeld, C. H., and Rai, C. S. (2011). "Transmission and scanning electron microscopy investigation of pore connectivity of gas shales on the nanoscale," in *Proceedings of the North American Unconventional Gas Conference and Exhibition*, Woodlands, TX, 14–16. doi: 10.2118/144391-MS

De, B. J. H. (1958). "The shape of capillaries," in *The Structure and Properties of Porous Materials*, eds D. H. Evertt and F. S. Stone (London: Butterworths), 68–94.

Dewhurst, D. N., Aplin, A. C., and Sarda, J. P. (1999). Influence of clay fractionon pore-scale properties and hydraulic conductivity of experimentally compacted mudstones. *J. Geophys. Res. Atmos.* 104, 29261–29274. doi: 10.1029/1999JB900276

Dong, D. Z., Gao, S. K., Huang, J. L., Guan, Q. Z., Wang, S. F., and Wang, Y. M. (2014). A discussion on the shale gas exploration and development prospect in the Sichuan Basin. *Nat. Gas. Ind.* 34, 1–15. doi: 10.1016/j.ngib.2015.02.002

Dubinin, M. M. (1989). Fundamentals of the theory of adsorption inmicropores of carbon adsorbents: characteristics of their adsorption properties and microporous structures. *Carbon* 27, 457–467. doi: 10.1016/0008-6223(89)90078-X

Fang, Z. H., Huang, Z. L., Wang, Q. Z., Zheng, D. W., and Liu, H. L. (2014). Cause and significance of the ultra-low water saturation in gas-enriched shale reservoir. *Nat. Gas. Geosci.* 25, 471–476. doi: 10.11764/j.issn.1672-1926.2014.03.0471

Fu, C. Q. (2017). Study on shale reservoir characteristics and shale gas enrichment of Wufeng Formation and Longmaxi Formation in southeast Chongqing. *Chin. Uni. Min. Technol.* ***Q,

Gasparik, M., Bertier, P., Gensterblum, Y., Ghanizadeh, A., Krooss, B. M., and Littke, R. (2014). Geological controls on the methane storage capacity in organic-rich shales. *Int. J. Coal. Geol.* 123, 34–51. doi: 10.1016/j.coal.2013.06.010

Gasparik, M., Ghanizadeh, A., Bertier, P., Gensterblum, Y., Bouw, S., and Krooss, B. M. (2012). High-pressure methane sorption isotherms of black shales from The Netherlands. *Energy Fuel* 26, 4995–5004. doi: 10.1021/ef300405g

Gou, Q. Y., Xu, S., Hao, F., Zhang, B. Q., Shu, Z. G., Yang, F., et al. (2020). Quantitative calculated shale gas contents with different lithofacies: a case study of Fuling gas shale, Sichuan Basin, China. *J. Nat. Gas Sci. Eng.* 76:103222. doi: 10.1016/j.jngse.2020.103222

Gregg, S. J., and Sing, K. S. W. (1982). *Adsorption, Surface Area and Porosity*, 2nd Edn. New York, NY: Academic Press, 312. doi: 10.1524/zpch.1969.63.1_4.220

Guo, T. L. (2016). Discovery and characteristics of the fuling shale gas field and its enlightenment and thinking. *Earth Sci. Front.* 23, 29–43.

Hou, H. H., Shao, L. Y., Li, Y. H., Li, Z., Zhang, W. L., and Wen, H. J. (2018). The pore structure and fractal characteristics of shales with low thermal maturity from the Yuqia Coalfield, northern Qaidam Basin, North Western China. *Front. Earth Sci.* 12:148–159. doi: 10.1007/s11707-016-0617-y

Hu, C. L., Zhang, Y. F., Wang, Z. F., Li, J. J., and Zhang, H. B. (2014). Shale features and exploration prospect of shale gas in longmaxi formation in Northern Guizhou. *Special Oil Gas Reserv.* 21, 44–47.

Hu, H. Y., Hao, F., Lin, J. F., Lu, Y. C., Ma, Y. Q., and Li, Q. (2017). Organic matter-hosted pore system in theWufeng-Longmaxi (O_3w-S_1l) shale, Jiaoshiba area, Eastern Sichuan Basin, China. *Int. J. Coal. Geol.* 173, 40–50. doi: 10.1016/j.coal.2017.02.004

Hu, Z. M., Duan, X. G., He, Y. B., Wu, J. F., Chang, J., Liu, L., et al. (2018). Influence of reservoir primary water on shale gas occurrence and flow capacity. *Nat. Gas. Ind.* 38, 44–51.

Jarvie, D. M., Hill, R. J., Ruble, T. E., and Pollastro, R. M. (2007). Unconventional shale-gas systems: the Mississippian Barnett shale of north-central texas as one model for thermogenic shale-gas assessment. *AAPG Bull.* 91, 475–499. doi: 10.1306/12190606068

Ji, L. M., Zhang, T. W., Milliken, K. L., Qu, J. L., and Zhang, X. L. (2012). Experimental investigation of main controls to methane adsorption in clay-rich rocks. *Appl. Geochem.* 27, 2533–2545. doi: 10.1016/j.apgeochem.2012.08.027

Klewiah, I., Berawala, D. S., Walker, H. C. A., Andersen, P. O., and Nadeau, P. H. (2019). Review of experimental sorption studies of CO_2 and CH_4 in shales. *J. Nat. Gas Sci. Eng.* 73:103045. doi: 10.1016/j.jngse.2019.103045

Kozbial, A., Li, Z. T., Sun, J. N., Gong, X., Zhou, F., Wang, Y. J., et al. (2014). Understanding the intrinsic water wettability of graphite. *Carbon* 74, 218–225. doi: 10.1016/j.carbon.2014.03.025

Li, H. X., and Zhang, Y. W. (2015). Global shale gas exploration and development today and China's shale gas development strategy. *Sino Glob. Energy* 20, 22–29.

Li, J., Li, X. F., Wang, X. Z., Li, Y. Y., Shi, J. T., Feng, D., et al. (2016a). A quantitative model to determine water-saturation distribution characteristics inside shale inorganic pores. *Acta. Pet. Sin.* 37, 903–913. doi: 10.7623/syxb201607009

Li, J., Li, X. F., Wang, X. Z., Li, Y. Y., Wu, K. L., Shi, J. T., et al. (2016b). Water distribution characteristic and effect on methane adsorption capacity in shale clay. *Int. J. Coal. Geol.* 159, 135–154. doi: 10.1016/j.coal.2016.03.012

Li, J. L., Xie, R. Y., You, J. J., and Wang, L. F. (2012). Reservoir forming condition and exploration prospect of shale-gas in Guizhou qianbei area. *China Min. Mag.* 21, 55–59.

Li, Q. W., Pang, X. Q., Tang, L., Chen, G., Shao, X. H., Jia, N., et al. (2018). Occurrence features and gas content analysis of marine and continental shales: a comparative study of Longmaxi Formation and Yanchang Formation. *J. Nat. Gas Sci. Eng.* 56, 504–522. doi: 10.1016/j.jngse.2018.06.019

Li, S. (2018). "Evaluation of shallow shale gas potential in T Structure of Zhaotong demonstration area. Natural gas professional committee of the China petroleum society," in *Proceedings of the 2018 National Natural Gas Academic Annual Conference (03 Unconventional Gas Reservoirs)*, 153–159. doi: 10.26914/c.cnkihy.2018.002595

Liang, D. G., Guo, T. L., Chen, J. P., Bian, L. Z., and Zhao, Z. (2008). Some progresses on studies of hydrocarbon generation and accumulation in marine sedimentary regions, Southern China (Part 1): distribution of four suits of regional marine source rocks. *Mar. Ori. Pet. Geol.* 13, 1–16.

Liang, X., Xu, Z. Y., Zhang, Z., Wang, W. X., Zhang, J. H., Lu, H. L., et al. (2020). Breakthrough of shallow shale gas exploration in Taiyang anticline area and its significance for resource development in Zhaotong, Yunnan province, China. *Pet. Exp. Dev* 47, 1–18.

Lin, W., Mastalerz, M., Schimmelmann, A., and Chen, Y. Y. (2014). Influence of soxhlet-extractable bitumen and oil on porosity in thermally maturing organic-rich shales. *Int. J. Coal. Geol.* 132, 38–50. doi: 10.1016/j.coal.2014.08.003

Liu, H. L., and Wang, H. Y. (2013). Ultra-low water saturation characteristics and thei dentification of over pressured play fairways of marine shales in South China. *Nat. Gas. Ind.* 33, 140–144. doi: 10.3787/j.issn.1000-0976.2013.07.025

Liu, X., Zhang, J. C., Liu, Y., Huang, H., and Liu, Z. Y. (2018). Main factors controlling the wettability of gas shales: a case study of over-mature marine shale in the Longmaxi Formation. *J. Nat. Gas Sci. Eng.* 56, 18–28. doi: 10.1016/j.jngse.2018.05.017

Löhr, S. C., Baruch, E. T., Hall, P. A., and Kennedy, M. J. (2015). Is organic pore development in gas shales influenced by the primary porosity and structure of

thermally immature organic matter? *Org. Geochem.* 87, 119–132. doi: 10.1016/j.orggeochem.2015.07.010

Mastalerz, M., Schimmelmann, A., Drobniak, A., and Chen, Y. Y. (2013). Porosity of devonian and mississippian New Albany Shale across a maturation gradient: insights from organic petrology, gas adsorption, and mercury intrusion. *AAPG Bull.* 97, 1621–1643. doi: 10.1306/04011312194

Newsham, K. E., Rushing, J. A., and Lasswell, P. M. (2003). Use of vapor desorption data to characterize high vapillary pressures in a basin-centered gas accumulation with ultra-low connate water saturations. *Paper Presented at the SPE Annual Technical Conference and Exhibition.* SPE-84596-MS, Denver, CO, 1–9. doi: 10.2118/84596-MS

Pan, L., Xiao, X. M., Tian, H., Zhou, Q., Chen, L., Li, T. F., et al. (2015). A preliminary study on the characterization and controlling factors of porosity and pore structure of the Permian shales in Lower Yangtze region, Eastern China. *Int. J. Coal Geol.* 146, 68–78. doi: 10.1016/j.coal.2015.05.005

Pan, L., Xiao, X., Tian, H., Zhou, Q., and Cheng, P. (2016). Geological models of gas in place of the Longmaxi shale in Southeast Chongqing, South China. *Mar. Pet. Geol.* 73, 433–444. doi: 10.1016/j.marpetgeo.2016.03.018

Pan, Z. J., and Connell, L. D. (2015). Reservoir simulation of free and adsorbed gas production from shale. *Nat. Gas Sci. Eng.* 22, 359–370. doi: 10.1016/j.jngse.2014.12.013

Ross, D. J. K., and Bustin, R. M. (2007). Shale gas potential of the Lower Jurassic Gordondale Member, northeastern British Columbia, Canada. *Bull. Can. Petrol. Geol.* 55, 51–75. doi: 10.2113/gscpgbull.55.1.51

Ross, D. J. K., and Bustin, R. M. (2009). The importance of shale composition and pore structure upon gas storage potential of shale gas reservoirs. *Mar. Pet. Geol.* 26, 916–927. doi: 10.1016/j.marpetgeo.2008.06.004

Rouquerol, J., Avnir, D., Fairbridge, C. W., Everett, D. H., Haynes, J. H., Pernicone, N., et al. (1994). Recommendations for the characterization of porous solids. *Pure Appl. Chem.* 66, 1739–1758. doi: 10.1351/pac199466081739

Shan, C. A., Zhang, T. S., Wei, Y., and Zhao, Z. (2017). Shale gas reservoir characteristics of Ordovician-Silurian formations in the central Yangtze area, China. *Front. Earth Sci.* 11:184–201. doi: 10.1007/s11707-016-0565-4

Sing, K. S. W., Everett, D. H., Haul, R. A. W., Moscou, L., Pierotti, R. A., Rouquerol, J., et al. (1985). Reporting physisorption data for gas/sold systems with special reference to the determination of surface area and porosity. *Pure. Appl. Chem.* 57, 603–619. doi: 10.1351/pac198557040603

Sondergeld, C. H., Ambrose, R. J., Rai, C. S., and Moncrieff, J. (2010). "Micro-structural studies of gas shales," in *Proceedings of the SPE Unconventional Gas Conference*, Pittsburgh, PA, 23–25. doi: 10.2523/131771-MS

Song, X., Wang, S. B., Cao, T. T., and Song, Z. G. (2013). The methane adsorption features of Cambrian shales in the Yangtze Platform. *Acta Geol. Sin* 87, 1041–1048.

Sun, J., Xiao, X. M., Wei, Q., Cheng, P., Tian, H., and Wu, Y. W. (2020). Gas in place and its controlling factors of the shallow Longmaxi shale in the Xishui area. Guizhou, China. *J. Nat. Gas. Sci. Eng.* 77:103272. doi: 10.1016/j.jngse.2020.103272

Tan, J. Q., Weniger, P., Krooss, B., Merkel, A., Horsfield, B., Zhang, J., et al. (2014). Shale gas potential of the major marine shale formations in the Upper Yangtze Platform, South China, Part II: methane sorption capacity. *Fuel* 129, 204–218. doi: 10.1016/j.fuel.2014.03.064

Tian, H., Li, T. F., Zhang, T. W., and Xiao, X. M. (2016). Characterization of methane adsorption on overmature Lower Silurian—Upper Ordovician shales in Sichuan Basin, southwest China: experimental results and geological implications. *Int. J. Coal. Geol.* 156, 36–49. doi: 10.1016/j.coal.2016.01.013

Tian, G. (2018). Zhejiang Oilfield of Petrochina Company has achieved breakthrough in shallow shale gas field. *Nat. Gas. Ind.* 38:40.

Tian, H., Pan, L., Xiao, X. M., Wilkins, R. W. T., Meng, Z. P., and Huang, B. J. (2013). A preliminary study on thepore characterization of Lower Silurian black shales in the Chuandong Thrust Fold Belt, southwestern China using low pressure N_2 adsorption and FE-SEM methods. *Mar. Petrol. Geol.* 48, 8–19. doi: 10.1016/j.marpetgeo.2013.07.008

Tian, H., Pan, L., Zhang, T. W., Xiao, X. M., Meng, Z. P., and Huang, B. J. (2015). Pore characterization of organic-rich lower Cambrian shales in Qiannan depression of Guizhou province, southwestern China. *Mar. Petrol. Geol.* 62, 28–43. doi: 10.1016/j.marpetgeo.2015.01.004

Wang, F. (2012). "Unique shale properties and their impacts on fluid flow-"Advances in shale"," in *Oral Presentation at State Key Laboratory of Org Geochem* (Guangzhou: Chinese Academy of Sciences).

Wang, F. T., and Guo, S. B. (2019). Shale gas content evolution in the Ordos Basin. *Int. J. Coal. Geol.* 211:103231. doi: 10.1016/j.coal.2019.103231

Wang, L., Wang, D. B., Cai, C. H., Li, N., Zhang, L., and Yang, M. L. (2020). Effect of water occupancy on the excess adsorption of methane in montmorillonites. *J. Nat. Gas. Sci. Eng.* 80:103393. doi: 10.1016/j.jngse.2020.103393

Wei, Y. Y., and Jia, C. Q. (2015). Intrinsic wettability of graphitic carbon. *Carbon* 87, 10–17. doi: 10.1016/j.carbon.2015.02.019

Wei, Z. H., and Wei, X. F. (2014). Comparison of gas-bearing property between different pore types of shale: a case from the Upper Ordovician Wufeng and Longmaxi formation in the Jiaoshiba area, Sichuan Basin. *Nat. Gas Ind.* 34, 37–41. doi: 10.3787/j.issn.1000-0976.2014.06.006

Yaguzhinsky, L. S., Motovilov, K. A., Volkov, E. M., Hu, Z. M., Liu, H. L., and Yu, R. Z. (2013). Impact of temperature on the isothermal adsorption/desorption characteristics of shale gas. *Pet. Explor. Dev.* 40, 514–519.

Yang, B. H. (2018). Zhejiang oilfield: towards to the shallow shale gas development. *Petrol. Knowl.* 22.

Yang, Y., and Aplin, A. C. (1998). Influence of lithology and compaction onthe pore size distribution and modelled permeability of some mudstones from the Norwegian margin. *Mar. Petrol. Geol.* 15, 163–175. doi: 10.1016/S0264-8172(98)00008-7

Ye, Z. H., Chen, D., Pan, Z. J., Zhang, G. Q., Xia, Y., and Ding, X. (2016). An improved Langmuir model for evaluating methane adsorption capacity in shale under various pressures and temperatures. *J. Nat. Gas. Sci. Eng.* 31, 658–680. doi: 10.1016/j.jngse.2016.03.070

Zhang, H., Zhu, Y. M., Xia, X. H., Lin, H., and Chen, J. (2013). Comparison and explanation of the absorptivity of organic matters and clay minerals in shales. *J. Chin. Coal. Soc.* 38, 812–816.

Zhang, T. W., Ellis, G. S., Ruppel, S. C., Milliken, K., and Yang, R. S. (2012). Effect of organic-matter type and thermal maturity on methane adsorption in shale-gas systems. *Org. Geochem.* 47, 120–131. doi: 10.1016/j.orggeochem.2012.03.012

Zhang, Y. F., Yu, B. S., Pan, Z. J., Hou, C. H., Zuo, Q. W., and Sun, M. D. (2020). Effect of thermal maturity on shale pore structure: a combined study using extracted organic matter and bulk shale from Sichuan Basin, China. *J. Nat. Gas Sci. Eng.* 74:103089. doi: 10.1016/j.jngse.2019.103089

Zhang, Y. S., Lv, D. W., Wang, Y., Liu, H. Y., Song, G. Z., Gao, J., et al. (2020). Geological characteristics and abnormal pore pressure prediction in shale oil formations of the Dongying depression, China. *Energy Sci. Eng.* 8, 1962–1979. doi: 10.1002/ese3.641

Conflict of Interest: The authors declare that the research was conducted in the absence of any commercial or financial relationships that could be construed as a potential conflict of interest.